

| | | |
|--|----------------------------------|--|
| 1. REPORT NUMBER CA15-2493 | 2. GOVERNMENT ASSOCIATION NUMBER | 3. RECIPIENT'S CATALOG NUMBER |
| 4. TITLE AND SUBTITLE Interaction of GRS Abutments with Bridge Superstructures under Seismic Loading Phase I | | 5. REPORT DATE April 2, 2015 |
| | | 6. PERFORMING ORGANIZATION CODE |
| 7. AUTHOR Patrick J. Fox, P. Benson Shing, and Yewei Zheng | | 8. PERFORMING ORGANIZATION REPORT NO. UCSD/SSRP 15-01 |
| 9. PERFORMING ORGANIZATION NAME AND ADDRESS Division of Structural Engineering School of Engineering University of California, San Diego La Jolla, California 92093-0085 | | 10. WORK UNIT NUMBER |
| | | 11. CONTRACT OR GRANT NUMBER 65A0483 |
| 12. SPONSORING AGENCY AND ADDRESS California Department of Transportation Division of Research and Innovation (MS-83) P.O. Box 942873 Sacramento, CA 94273-0001 | | 13. TYPE OF REPORT AND PERIOD COVERED Final Report |
| | | 14. SPONSORING AGENCY CODE |

15. SUPPLEMENTARY NOTES
 Prepared in cooperation with the State of California Department of Transportation

16. ABSTRACT
 This report summarizes the findings of a Phase I investigation of the seismic performance of geosynthetic-reinforced soil (GRS) bridge abutments. For this application, the bridge load is directly applied to the reinforced soil backfill through a shallow foundation. This concept represents significant cost savings through the avoidance of deep foundations (piles) and provides several other advantages. Research is needed to address a variety of issues before MSE abutments can be used to full advantage in high seismic areas. A literature review is presented on static and dynamic analyses of MSE retaining walls and bridge abutments and observations from post-earthquake field reconnaissance studies. Numerical studies were conducted using FLAC-2D (finite difference) and ABAQUS (finite element) software packages. FLAC was validated for static analysis using published field measurements for the Founders/Meadows GRS bridge abutment in Colorado. Numerical simulations were then conducted using FLAC and ABAQUS to predict settlement and lateral displacement for a GRS abutment in the Northridge earthquake and showed good agreement. Numerical simulation results were also compared with measured data for shaking table tests of a field-scale MSE wall on the UCSD large outdoor shake table. Numerical results for this latter study indicated that FLAC substantially overestimated wall displacement measurements for this large-scale test. Numerical simulations were conducted using FLAC to study the seismic response of GRS abutments supporting a 150 ft. bridge during the Northridge earthquake with ground motion applied in both the longitudinal and transverse directions. Parametric studies were carried out to investigate the effects of several design parameters, including reinforcement spacing, reinforcement stiffness, reinforcement length, soil cohesion, soil friction angle, bridge load, earthquake ground motion record, and bearing pad friction coefficient on the seismic response of GRS abutments in the longitudinal direction. The effect of soil shear keys to reduce seismic-induced lateral movement of a bridge seat in the transverse direction was also investigated. Numerical results indicate that seismic-induced settlements of a bridge seat on a GRS abutment were small, approximately 0.65 in., for the Northridge-Newhall Station ground motion record. Corresponding seismic-induced lateral displacements of the bridge seat were 2.5 in. or less. Reinforcement stiffness and soil cohesion had a large influence on these displacements. Soil shear keys were shown to be effective in reducing lateral displacement of the bridge seat in the transverse direction. Results from this Phase I investigation suggest that GRS bridge abutments are a viable option for single-span and multi-span bridges in California.

| | |
|--|---|
| 17. KEY WORDS Geosynthetic reinforced soil, abutment, seismic, numerical modeling | 18. DISTRIBUTION STATEMENT No restrictions. This document is available to the public through the National Technical Information Service, Springfield, VA, 22161. |
|--|---|

| | | |
|--|---------------------------|----------------------------|
| 19. SECURITY CLASSIFICATION (of this report) Unclassified | 20. NUMBER OF PAGES 87 | 21. COST OF REPORT CHARGED |
|--|---------------------------|----------------------------|

DISCLAIMER

This document is disseminated in the interest of information exchange. The contents of this report reflect the views of the authors who are responsible for the facts and accuracy of the data presented herein. The contents do not necessarily reflect the official views or policies of the State of California or the Federal Highway Administration. This publication does not constitute a standard, specification or regulation. This report does not constitute an endorsement by the California Department of Transportation of any product described herein.

For individuals with sensory disabilities, this document is available in Braille, large print, audiocassette, or compact disk. To obtain a copy of this document in one of these alternate formats, please contact: the Division of Research and Innovation, MS-83, California Department of Transportation, P.O. Box 942873, Sacramento, CA 94273-0001.



**STRUCTURAL SYSTEMS
RESEARCH PROJECT**

Report No.
SSRP 15-01

**Interaction of GRS Abutments with Bridge
Superstructures under Seismic Loading
Phase I**

by

Patrick J. Fox

P. Benson Shing

Yewei Zheng

Report Submitted to the California Department of Transportation
under Contract No. 65A0483

April 2015

Department of Structural Engineering
University of California, San Diego
La Jolla, California 92093-0085

University of California, San Diego
Department of Structural Engineering
Structural Systems Research Project

Report No. SSRP 15-01

Interaction of GRS Abutments with Bridge Superstructures under Seismic Loading

by

Patrick J. Fox, Ph.D., P.E.
Professor of Structural Engineering

P. Benson Shing, Ph.D.
Professor of Structural Engineering

Yewei Zheng
Graduate Research Assistant

Final Report Submitted to the California Department of Transportation
under Contract No. 65A0483

Department of Structural Engineering
University of California, San Diego
La Jolla, California 92093-0085

April 2015

ACKNOWLEDGEMENTS

This work was supported by the California Department of Transportation under Agreement #65A0483. The authors sincerely thank the project liaison, Dr. Charles Sikorsky, for his assistance with this project, and Andrew Sander for his contribution to some of the work in this report.

ABSTRACT

This report summarizes the findings of a Phase I investigation of the seismic performance of geosynthetic-reinforced soil (GRS) bridge abutments. For this application, the bridge load is directly applied to the reinforced soil backfill through a shallow foundation. This concept represents significant cost savings through the avoidance of deep foundations (piles) and provides several other advantages. Research is needed to address a variety of issues before MSE abutments can be used to full advantage in high seismic areas like California.

A literature review is presented on static and dynamic analyses of MSE retaining walls and bridge abutments and observations from post-earthquake field reconnaissance studies. Numerical studies were conducted using FLAC-2D (finite difference) and ABAQUS (finite element) software packages. FLAC-2D was validated for static analysis using published field measurements for the Founders/Meadows GRS bridge abutment in Denver, Colorado. Numerical simulations were then conducted using FLAC-2D and ABAQUS to predict settlement and lateral displacement for a GRS abutment subjected to the Newhall Station ground motion record from the 1994 Northridge earthquake and showed good agreement. Numerical simulation results were also compared with measured data for seismic tests of a field-scale MSE wall on the UCSD large outdoor shake table. Numerical results for this latter study indicated that FLAC-2D overestimated wall displacement measurements for this large-scale test.

Numerical simulations were conducted using FLAC-2D to study the seismic response of GRS abutments supporting a 150 ft. bridge for the Northridge record with ground motion applied in both the longitudinal and transverse directions. Parametric studies were carried out to investigate the effects of several design parameters, including reinforcement spacing, reinforcement stiffness, reinforcement length, soil cohesion, soil friction angle, bridge load, earthquake ground motion record, and bearing pad friction coefficient on the seismic response of GRS abutments in the longitudinal direction. The effectiveness of soil shear keys to reduce seismic-induced lateral movement of a bridge seat in the transverse direction was also investigated. Numerical results indicate that seismic-induced settlements of a bridge seat on a GRS abutment were small, approximately 0.65 in., for the Northridge-Newhall Station ground motion record. Corresponding seismic-induced lateral displacements of the bridge seat were 2.5 in. or less. Reinforcement stiffness and soil cohesion had a large influence on these displacements. Soil shear keys were shown to be effective in reducing lateral displacement of the bridge seat in the transverse direction.

Results from this Phase I investigation suggest that GRS bridge abutments may be a viable option for single-span and multi-span bridges in California. Based on these numerical results, shake table testing of GRS bridge abutments is the next logical step to evaluate the seismic performance of this design concept for Caltrans.

TABLE OF CONTENTS

| | |
|--|----|
| Chapter 1 – Introduction..... | 1 |
| Chapter 2 – Background..... | 3 |
| 2.1 MSE Bridge Abutment Structures..... | 3 |
| 2.2 Performance of Retaining Walls during Earthquakes..... | 5 |
| 2.3 Performance of MSE Walls during 2010 Maule Earthquake, Chile..... | 5 |
| Chapter 3 – Literature Review..... | 8 |
| 3.1 Static Analysis of Geosynthetic-Reinforced Soil (GRS) Retaining Walls..... | 8 |
| 3.1.1 Experimental Studies..... | 8 |
| 3.1.2 Numerical Studies..... | 9 |
| 3.1.2.1 Finite Element Method..... | 9 |
| 3.1.2.2 Finite Difference Method..... | 11 |
| 3.2 Dynamic Analysis of Geosynthetic-Reinforced Soil (GRS) Retaining Walls..... | 13 |
| 3.2.1 Experimental Studies..... | 13 |
| 3.2.1.1 Shaking Table Tests..... | 13 |
| 3.2.1.2 Dynamic Centrifuge Tests..... | 16 |
| 3.2.2 Numerical Studies..... | 17 |
| 3.2.2.1 Finite Element Method..... | 17 |
| 3.2.2.2 Finite Difference Method..... | 19 |
| 3.3 Static Analysis of Geosynthetic-Reinforced Soil (GRS) Bridge Abutments..... | 19 |
| 3.3.1 Experimental Studies..... | 19 |
| 3.3.1.1 Field Project Instrumentation and Monitoring..... | 19 |
| 3.3.1.2 Field Loading Tests..... | 21 |
| 3.3.2 Numerical Studies..... | 24 |
| 3.4 Dynamic Analysis of Geosynthetic-Reinforced Soil (GRS) Bridge Abutments..... | 25 |
| 3.4.1 Experimental Studies..... | 25 |
| 3.4.2 Numerical Studies..... | 26 |
| Chapter 4 – Research Tasks..... | 27 |
| Chapter 5 – Validation of FLAC for Static Analysis of GRS Bridge Abutment..... | 28 |
| 5.1 Description of the Founders/Meadows GRS Bridge Abutment..... | 28 |
| 5.2 Numerical Model..... | 29 |
| 5.2.1 Finite Difference Grid and Boundary Conditions..... | 29 |
| 5.2.2 Material Models and Properties..... | 30 |
| 5.3 Simulation Results..... | 31 |
| 5.3.1 Key Deformations of GRS Bridge Abutment..... | 31 |
| 5.3.2 Geogrid Strains..... | 33 |

| | |
|--|--------|
| 5.3.3 Lateral Earth Pressures..... | 34 |
| 5.3.4 Vertical Stresses..... | 35 |
| 5.4 Summary..... | 37 |
| Chapter 6 – Numerical Simulations of GRS Retaining Wall for Seismic Loading..... | 39 |
| 6.1 UCSD Shaking Table Test..... | 39 |
| 6.2 Numerical Simulations..... | 40 |
| 6.3 Simulation Results..... | 41 |
| 6.4 Summary..... | 41 |
| Chapter 7 – Numerical Simulations of Seismic Response of GRS Abutments in Longitudinal Direction..... | 42 |
| 7.1 Numerical Model..... | 42 |
| 7.1.1 Model Geometry..... | 42 |
| 7.1.2 Material Models and Properties..... | 43 |
| 7.2 Static Analysis..... | 44 |
| 7.3 Seismic Analysis..... | 44 |
| 7.4 Simulation Results for Base Case..... | 45 |
| 7.5 Parametric Studies..... | 45 |
| 7.5.1 Reinforcement Spacing..... | 46 |
| 7.5.2 Reinforcement Stiffness..... | 47 |
| 7.5.3 Reinforcement Length..... | 48 |
| 7.5.4 Soil Cohesion..... | 49 |
| 7.5.5 Soil Friction Angle..... | 50 |
| 7.5.6 Bridge Load..... | 51 |
| 7.5.7 Earthquake Ground Motion Record..... | 52 |
| 7.5.7 Bridge Bearing Pad Friction Coefficient..... | 53 |
| 7.6 Summary..... | 56 |
| Chapter 8 – Comparison of FLAC and ABAQUS Results for Seismic Response of GRS Bridge Abutments in Longitudinal Direction..... | 58 |
| 8.1 Numerical Model..... | 58 |
| 8.1.1 Model Geometry..... | 58 |
| 8.1.2 Numerical Meshes and Boundary Conditions..... | 59 |
| 8.1.3 Material Models and Properties..... | 59 |
| 8.2 Modeling Procedures..... | 59 |
| 8.3 Results..... | 60 |
| 8.4 Summary..... | 62 |

| | |
|---|--------|
| Chapter 9 – Numerical Simulations of Seismic Response of GRS Abutments in Transverse Direction..... | 63 |
| 9.1 Numerical Model..... | 63 |
| 9.1.1 Model Geometry..... | 63 |
| 9.1.2 Material Models and Properties..... | 64 |
| 9.2 Static Analysis..... | 64 |
| 9.3 Seismic Analysis..... | 65 |
| 9.4 Simulation Results | 65 |
| 9.6 Summary..... | 66 |
| Chapter 9 – Conclusions..... | 67 |
| References..... | 69 |

Chapter 1 – Introduction

This report summarizes the findings of a Phase I investigation of the seismic performance of mechanically stabilized earth (MSE) bridge abutments. Developed in the late 1960s and 1970s, MSE is an established technology and has been used in transportation infrastructures across the U.S. with an excellent service record spanning several decades. With regard to bridge structures, MSE has typically been used for retaining walls that support the on-ramp but not the bridge itself. However, more recently, MSE is being considered for bridge abutments in place of conventional abutment structures. Potential advantages of this approach include: 1) simplified design and construction, 2) faster construction, 3) better performance under differential foundation settlement, 4) better settlement compatibility between bridge and approach ramp, and 5) lower construction and maintenance costs. In particular, the use of MSE can eliminate deep foundations (piles) under bridge abutments and thereby provide considerable cost savings during construction.

Post-earthquake reconnaissance studies indicate that MSE walls have generally performed well under seismic conditions (Koseki 2012). In some cases, failure has been attributed to a lack of seismic design (Ling et al. 2001); however, in most cases failure during earthquakes resulted from design or construction flaws that were not associated with strong shaking (Yen et al. 2011). In general, wall performance problems during shaking occur for high accelerations or when poor foundation soils are present on a site. As such, the current AASHTO requirements for seismic design of MSE walls are limited to one or more of the following conditions: 1) accelerations $\geq 0.4g$, 2) walls located in Seismic Zone 4, 3) potentially liquefiable or otherwise sensitive foundation soils, 4) walls that support another structure, 5) walls with height ≥ 30 ft., 6) walls with abrupt changes in alignment, and 7) walls with low quality soil backfills.

Considering the above trends, it is clear that designers are gaining confidence in the seismic performance of MSE walls for transportation applications. The next step is the adaptation of MSE technology for bridge abutments – which is a more serious application. In this case, the bridge load is directly applied to the reinforced soil backfill through a shallow foundation. This represents a significant cost savings through the avoidance of deep foundations for the bridge abutments. The “bump at the end of the bridge” problem is also avoided because the bridge settles with the backfill for the on-ramp. This settlement will generally not be problematic for simply supported bridge structures. For multi-span bridges with one or more internal supports, such settlement may or may not be problematic depending on the induced stresses in the bridge. Several investigations have been conducted on the use of this type of “true” MSE abutment for bridge support and have generally reported positive results (e.g., Zornberg et al. 2001; Zevgolis and Bourdeau 2007; Tatsuoka 2008; Lostumbo and Artieres 2011).

Although good performance of true MSE abutments has been demonstrated for static loading, much less is known with regard to their performance under seismic conditions. For example, the performance of only one true MSE bridge abutment was reported (out of 32 sites) during the recent 2010 Maule Earthquake in Chile (Yen et al. 2011). Reconnaissance observations indicated that this wall performed well; however no quantitative measurements are available to develop seismic design guidelines. Thus, much remains to be learned regarding the seismic behavior of these potentially important structures, including:

- Forces on facing elements
- Maximum tensile loads in soil reinforcement
- Optimal layout of reinforcement
- Equivalent values for shear modulus and damping ratio of completed abutment
- Shaking-induced settlement and differential settlement of reinforced backfill
- Interaction of bridge superstructure with MSE abutment
- Permanent wall deflections

Research is needed to address these issues before MSE abutments can be used to their full advantage in high seismic areas like California.

A comprehensive two-phase research program has been proposed to investigate the seismic performance of MSE bridge abutments and develop guidelines for seismic design of these structures. Phase I has consisted of literature review and analytical/numerical studies, leading up to shake table tests for Phase II. Phase II is envisioned to consist of shake table tests of six reduced-scale (2.5 m tall) MSE bridge abutments. The abutments will be shaken in the longitudinal and/or transverse directions with superstructure loads applied during shaking. This report presents our findings for Phase I. Based on these results, a Phase II proposal was submitted during fall 2014, with Phase II work starting in summer 2015. The research program will provide one of first complete studies on the seismic performance of MSE abutments and is expected to provide Caltrans engineers with necessary data and guidelines to write specifications for MSE abutments for single-span and multi-span bridge structures with lengths of 150 ft. and more.

Chapter 2 – Background

2.1 MSE Bridge Abutment Structures

Mechanically stabilized earth (MSE) walls, also known as reinforced soil walls, are a special type of earth retaining structure composed primarily of the three elements: 1) soil backfill, which is typically granular, 2) reinforcement, which can be metallic or geosynthetic, 3) and facing units. In principle, MSE retaining walls can be considered as composite structures where the earth fill stability and capacity to retain backfill are greatly improved by the reinforcements (Vidal 1969; Lee et al. 1973; Ingold 1982). The tensile capacity of the reinforcement provides additional internal confinement and shear strength that are naturally lacking in granular soil. Depending on the type of reinforcement, stresses are transferred between backfill soil and reinforcement through interface friction, passive resistance of interface particles, or a combination of both (Schlosser and Elias 1979; Schlosser and Bastick 1991). More than thirty years after their introduction in civil engineering, MSE structures have become widely accepted as an attractive alternative to traditional reinforced concrete retaining walls. In comparison to traditional walls, they are often more economical and, due to their inherent flexibility, can tolerate relatively large differential settlements without excessive structural distress (Mitchell and Christopher 1990; Jones 1996).

MSE walls have been extensively used for lateral support of highway embankment fills or access ramps, and more recently as bridge abutments. There are two types of bridge abutments that incorporate MSE walls (Jones 1996; Anderson and Brabant 2005). The first, called a mixed or “false” MSE abutment, is a pile-supported abutment where the reinforced soil wall provides lateral support to the approach embankment but not to the bridge itself. The piles are installed first and then the MSE structure is constructed around the piles. This type of design has shortcomings: the construction process is complicated, the cost is increased by the use of deep foundations, downdrag forces can develop on the piles, and differential settlements can occur between the approach embankment and the bridge. These problems can be avoided or minimized if the reinforced soil structure is designed not only to retain the approach embankment but also to support the bridge. In this second type of design, the bridge is supported by a shallow footing that rests directly on the reinforced soil mass. In this case, called a “true” MSE abutment, the reinforced soil wall must be designed to sustain not only the soil pressure but also the superstructure loads.

MSE structures can be built using inextensible (i.e., metallic) reinforcement, such as galvanized strips or welded wire mats, or with extensible (i.e., geosynthetic) reinforcement such as geotextiles or geogrids. This latter category is termed geosynthetic-reinforced soil (GRS) and is most commonly constructed using geogrid. Depending on the type of wall, facing elements can be either precast concrete panels or smaller concrete modular blocks. The backfill is generally recommended to be a clean granular soil with low fines content. In practice, MSE structures are

designed using limit equilibrium methods and classical soil plasticity theories (i.e., Coulomb and Rankine methods) combined with empirical knowledge gained from tests on small-scale models or full-scale prototypes. Numerical models using the finite difference method or finite element method are often used for research purposes as these models allow for predictions of detailed structure response, including distributions of stress and strains in the soil, pressures on the facing, and tensile forces in the reinforcement.

Figure 2.1 shows an example of a true GRS abutment. The abutment blends the roadway approach into the bridge superstructure to create a jointless interface that is generally expected to experience little to no differential settlement. The structure consists of several components: the reinforced soil foundation, abutment, bearing bed, integrated approach, and facing elements. The foundation is composed of compacted granular fill and may be encapsulated with a geotextile fabric. This low-cost foundation provides embedment and increases the bearing capacity for the structure. The GRS structure uses alternating layers of compacted fill and reinforcement to provide support for the bridge, which is placed directly on the bearing bed. The bearing bed contains more closely spaced reinforcement to strengthen the area that directly carries the bridge load. The integrated approach is also composed of reinforced soil and provides a jointless transition between the pavement and the bridge. The facing elements at the front of the wall carry only light vertical loads and are designed to resist the lateral pressure from the soil and the applied bridge load (Adams et al. 2011).

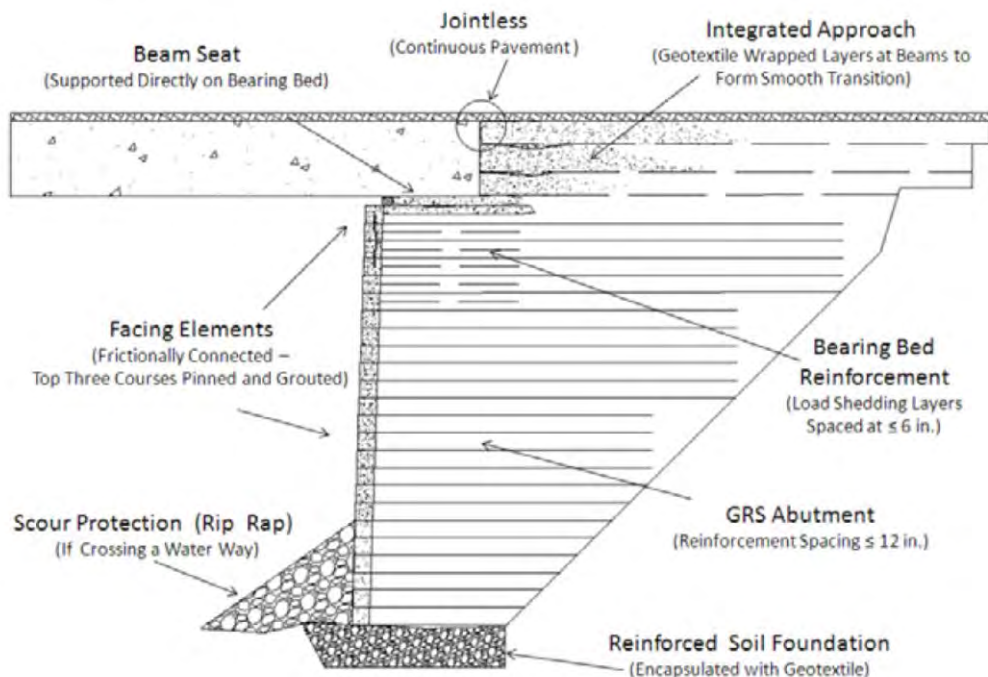


Figure 2.1. Example cross section of a “true” MSE bridge abutment (Adams et al. 2011).

2.2 Performance of Retaining Walls during Earthquakes

In general, retaining walls have performed well during earthquakes. Examples include soil nail walls and MSE walls in the 1989 Loma Prieta earthquake, MSE walls in the 1994 Northridge earthquake, and MSE walls and modern reinforced concrete gravity walls in the 1995 Kobe earthquake (Vucetic et al. 1998; Collin et al. 1992; Bathurst and Cai 1995; Tatsuoka et al. 1996). Koeski et al. (2006) also provided a summary of the performance of various types of retaining walls, focusing on GRS structures, in these and more recent earthquakes. The largest earthquakes have shown some differences in performance between relatively rigid walls such as concrete gravity walls and more flexible MSE-type walls, with the MSE structures tending to outperform the rigid structures, especially older concrete gravity walls. While some damage to MSE walls has occurred during earthquakes, the damage has typically been limited to small movements (4 in. or less), outward tipping of the wall, cracking of wall facing elements, wall corners or full-height joints opening up and allowing backfill to spill through, unsecured blocks toppling off the top, and on rare occasions, complete collapse. Instances of wall collapse were almost always limited to older walls that would not meet current seismic design standards and, in a few cases, newer walls that were not designed to standards or were already in serious distress before the earthquake due to design or construction problems (Yen et al. 2011).

2.3 Performance of MSE Walls during 2010 Maule Earthquake, Chile

Yen et al. (2011) published a detailed post-earthquake reconnaissance report for the very strong Maule earthquake that occurred in Chile on February 27, 2010. The Maule earthquake measured M8.8, lasted more than 2 minutes, and was approximately 500 times more powerful than the earthquake that devastated Haiti the previous month. Several aftershocks, including nine larger than M6.0, occurred in the days following the Maule earthquake. The main shock is the fifth largest earthquake recorded in modern times and was characterized by its long duration and strong ground motion, which also caused tsunamis across the region. Many bridges and tunnels constructed with seismic design codes similar to the 1983 U.S. and European codes were damaged in the earthquake. The performance of retaining walls was also assessed by the reconnaissance team.

Cast-in-place (CIP) and MSE retaining walls were observed at 14 sites visited by Maule earthquake reconnaissance team. Only one of these walls was a true MSE bridge abutment. The majority of walls performed very well and showed no signs of distress due to the earthquake, even though some of the bridges associated with these walls experienced significant damage or even complete collapse. Walls at 5 locations experienced deformations or damage, which was generally minor and repairable. These walls continued to perform their function of retaining soil and maintaining grade separation and should be able to be placed back into service after minor to moderate rehabilitation. Of the walls that deformed laterally, movement tended to be greatest near the wall top with little, if any, lateral movement at the base, indicating that resistance to sliding was likely greater than assumed in design. The most significant wall performance

problems were primarily caused by inadequate details at the corners and full-height joints and at the wall top due to inadequate coping connections. In spite of these performance problems, all of the walls met the no-collapse criterion typically applied for seismic design, including walls that were subjected to liquefaction of the foundation.

One of the damaged MSE walls, located at the Muros Talca site, is shown in Figure 2.2. This wall is approximately 30 ft. (9 m) high with a 1.5H:1V to 2H:1V unreinforced slope on top, and is adjacent to a CIP concrete abutment wall that supports the bridge. The wall experienced severe cracking of the facing blocks (along 45° angles), an outward lateral deformation of approximately 4 in., and formed a 4 to 6 in. gap with the CIP abutment. The opposite wall (not shown) also had some cracked blocks with a similar pattern but to a lesser degree. In this case, the wall height combined with the soil surcharge, a tight radius in wall alignment, and extreme seismic loading caused a severe demand on the facing blocks (Yen et al. 2011).



Figure 2.2. MSE wall at Muros Talca site showing deformations, permanent lateral displacement, and severe block cracking after 2010 Maule earthquake (Yen et al. 2011).

The only true MSE abutment investigated after the Maule earthquake, located at the Estribo Francisco Mostazal site, is shown in Figure 2.3. This geogrid-reinforced modular block wall is approximately 23 ft. (7 m) high and directly supports the bridge foundation load. The abutment performed very well, exhibiting no signs of lateral or vertical movement due to the earthquake. While the bridge suffered some relatively minor damage, the damage was not caused by the walls but was probably due to the severe bridge skew angle combined with the bridge tending to slide down hill, as it was located on a downhill roadway grade (Yen et al. 2011).



Figure 2.3. MSE bridge abutment at Estribo Francisco Mostazal site after 2010 Maule earthquake (Yen et al. 2011).

MSE walls in general and the one true MSE abutment in particular performed well during the 2010 Maule earthquake, which suggests that further research directed toward seismic performance characterization and the development of seismic design guidelines for these structures is warranted. The Maule earthquake reconnaissance team reached the same conclusion and provided the following summary statement and recommendation in their report (Yen et al. 2011):

“Bridges supported on MSE walls also appeared to have performed well in this earthquake. It is recommended that this cost-effective technology be investigated as an alternative to conventional, CIP, reinforced concrete abutment walls.”

Chapter 3 – Literature Review

3.1 Static Analysis of Geosynthetic-Reinforced Soil (GRS) Retaining Walls

3.1.1 Experimental Studies

Full-scale model tests with detailed instrumentation can be used to provide better understanding of the behavior of GRS structures. The geotechnical research group at the Royal Military College (RMC) of Canada has conducted a series of full-scale GRS retaining wall model tests since 1987. This long-term research program studied the behavior of GRS retaining walls during construction, under working stresses, and under surcharge loads approaching failure. The influences of different factors, such as reinforcement spacing, reinforcement stiffness, wall facing batter and wall facing rigidity, were also investigated.

The full-scale GRS retaining wall facility at RMC is shown in Figure 3.1. Figure 3.2 shows the cross-section of a typical GRS retaining wall test using this facility. This GRS retaining wall was 3.6 m high and 2.4 m wide, and was constructed by lifts on a concrete foundation. The geogrid reinforcement was placed at appropriate elevations during construction. For some tests, a uniform surcharge was applied on top surface using a large air bag.

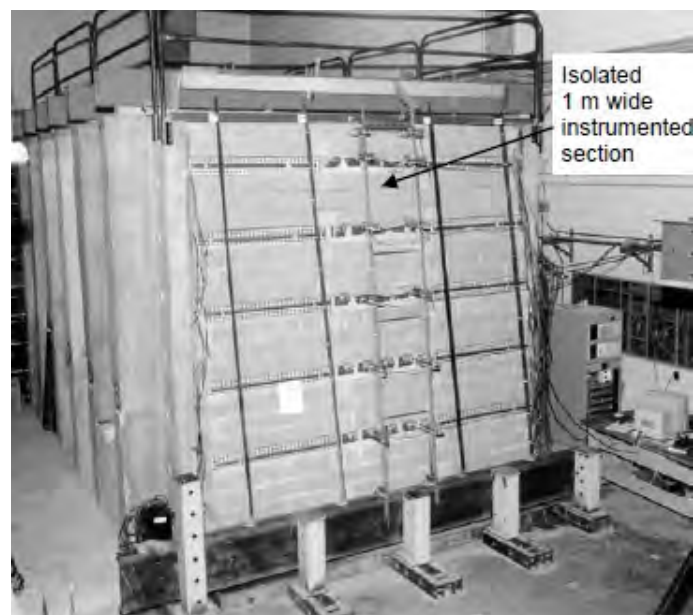


Figure 3.1. Full-scale GRS retaining wall facility at RMC (Bathurst et al. 2000).

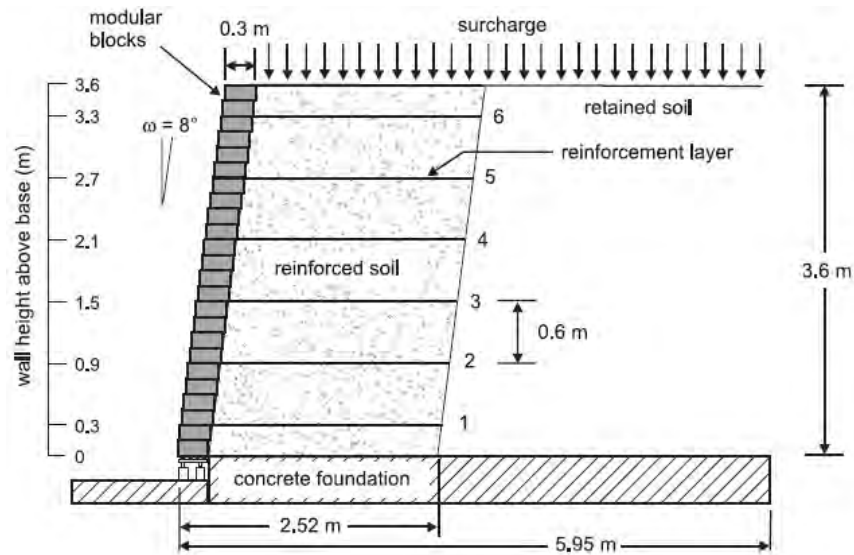


Figure 3.2. Typical cross-section of GRS retaining wall (Bathurst et al. 2006).

Bathurst et al. (2000) investigated the effects of reinforcement stiffness, reinforcement spacing, and wall facing type on the performance of GRS retaining walls. Four GRS wall models were constructed and loaded up to 115 kPa surcharge. The results indicate that lateral facing displacements can be reduced by increasing reinforcement stiffness or decreasing vertical reinforcement spacing. The toe of the walls was found to carry a significant portion of the total lateral earth force. Another series of 11 full-scale GRS wall tests were reported by Bathurst (2006), Bathurst et al. (2006), and Bathurst et al. (2009). In these studies, the effects of reinforcement type, reinforcement stiffness, reinforcement spacing, wall facing type, and wall facing batter were investigated. The results indicate that peak loads in the reinforcement for a wrapped-face wall were about 3.5 times larger than those for modular block face wall at the end of construction, and increased about 2 times under a surcharge load of 80 kPa. The modular block facing acted as a structural element that reduced wall deformations and reinforcement strains. For the GRS walls with modular block facing and incremental panel facing, connection loads were the largest in the reinforcement at the end of construction.

3.1.2 Numerical Studies

3.1.2.1 Finite Element Method

Bathurst et al. (1992) and Karpurapu and Bathurst (1995) simulated two full-scale GRS retaining walls with different facing conditions (incremental panel wall and full height panel wall) using finite element program GEOFOAM. A modified hyperbolic model that included soil dilation was used to simulate the behavior of sand during shearing. The reinforcement was modeled with uniaxial elements. Joint elements were used to simulate the interfaces between soil and reinforcement, and between soil and facing panels. All the parameters needed in the numerical simulations were determined from laboratory tests. Constant load tests were carried out to obtain

the strength and stiffness of reinforcement and interface shear tests were conducted to determine shear stiffness of different interfaces. Triaxial tests and direct shear tests were conducted to determine parameters for the modified Duncan-Chang soil model. The simulation results, including facing panel lateral displacements and reinforcement strains at the end of construction and under uniform surcharge loading, were compared with experimental results. They concluded that numerical simulations could accurately predict the performance of GRS walls at working stress levels and collapse conditions. They found that soil dilation was important in transferring load from reinforcement to soils during shearing, and it was necessary to consider soil dilatancy to accurately simulate the performance of GRS walls. Facing panel deformations and reinforcement strains could be over-predicted by a factor of two if soil dilation was not taken into account. Both the experimental observed and numerically predicted failure surfaces were in good agreement with the failure surface predicted using Rankine earth pressure theory.

Ho and Rowe (1996), and Rowe and Ho (1997, 1998) carried out parametric studies on GRS walls with continuous facing panels using the finite element program AFENA. In these studies, the effects of reinforcement properties, soil properties, interface friction angles, wall facing rigidity, and wall height were investigated. The backfill soil was modeled as an elasto-plastic material with a Mohr-Coulomb failure criterion and a non-associated flow rule. The reinforcement was modeled using linearly elastic bar elements with negligible compressive strength. Soil-reinforcement, soil-facing panel, and soil-foundation interfaces were modeled using joint elements with a Mohr-Coulomb failure criterion and zero dilation. The simulation results indicated that reinforcement stiffness, reinforcement length and soil friction angle are the most important parameters that influence the behavior of GRS walls with continuous facing. Other parameters, such as soil modulus, facing rigidity, soil-reinforcement friction angles and soil-facing panel friction angles are relatively less important. For a reinforcement length to wall height ratio, L/H , greater than 0.7, the influence of reinforcement length on the lateral facing displacement and reinforcement strains was very small, while the influence could be significant for a ratio less than 0.7. It is worth noting that the ratio L/H of 0.7 is the minimum value required by FHWA design guidelines (Berg et al. 2009). The design guidelines suggested that equally spaced reinforcement with $L/H = 0.7$ gives an efficient reinforcement distribution.

Helwany et al. (1999) verified their finite element model against measured results of the Denver Test Wall using program DACSAR. Soil behavior was simulated by the nonlinear elastic hyperbolic model with parameters determined from triaxial tests. The timber facing and geotextile reinforcement were modeled using linearly elastic beam elements and truss elements, respectively. Reasonable agreement was obtained between predicted and measured values of lateral facing displacements and reinforcement strains. They also investigated the influences of wall height, reinforcement stiffness and backfill soil type on the wall behavior under a uniform surcharge of 35 kPa. Backfill soil type was found to be the most important factor that influenced the performance of GRS walls. Reinforcement stiffness was also important when the backfill

soil stiffness and shear strength were low. Design charts were developed for selecting appropriate backfill soil type and reinforcement stiffness to satisfy performance requirements for GRS retaining walls.

Ling et al. (2000) used the finite element program M-CANDE to reproduce results of a fully instrumented full-scale model test on a GRS retaining wall during construction at the Public Works Research Institute (referred to as PWRI Wall). The PWRI Wall was 6 m high and 5 m wide, and reinforced with both primary geogrid (3.5 m) and secondary geogrid (1.0 m). In the numerical analysis, both the backfill soil and geosynthetic reinforcement were modeled using hyperbolic models. The hyperbolic models were calibrated using triaxial test and tensile test results for backfill soil and reinforcement, respectively. The block-block interface and soil-block interfaces were simulated using interface elements, and the interface friction angles and tensile strengths were determined from interface direct shear tests. Predicted results for lateral facing displacements, lateral and vertical stresses, and strains in reinforcement during construction were compared with measured results from a full-scale test. The comparison showed satisfactory agreement between predicted and measure results. Ling and Leshchinsky (2003) then carried out a parametric study with the validated model to investigate the effects of various design parameters on the behavior of GRS wall under working stress conditions. Lateral facing displacements and maximum tensile forces in the reinforcement increased with an increase in vertical reinforcement spacing. Lateral facing displacements decreased with increasing reinforcement stiffness, while the maximum tensile forces mobilized were the largest for the case with stiff reinforcement. For block-block interface friction angles greater than 20° , the variations for wall deformations and maximum reinforcement strains were negligible. Ling (2003) also compared simplistic and sophisticated finite element analyses for GRS retaining walls. Both the backfill soil and geosynthetic reinforcement were characterized using hyperbolic models in the simplistic analysis. However, in the sophisticated analysis, the backfill soil was modeled using a generalized plasticity model and the geogrid was simulated using a bounding surface model. Results for wall deformations, lateral and vertical stresses, and reinforcement strains from simplistic and sophisticated analyses were in good agreement, and both provided a reasonable match with measured results from a full-scale model test.

3.1.2.2 Finite Difference Method

A finite difference computer program FLAC (Itasca 2011) has been widely used to study the behavior of geosynthetic-reinforced soil structures under different loading conditions. Linear-elastic cable elements with a specified tensile yield strength can be used to model geosynthetic reinforcement, and interface elements characterized by interface friction angle and cohesion can be used model interactions between the different components of the complex GRS retaining wall system (soil, reinforcement, and concrete blocks).

Lee (2000) calibrated a FLAC model with monitored results from several fully instrumented full-scale GRS walls. He also carried out a parametric study to investigate the influences of soil properties, reinforcement properties, toe restraint, and facing type on the performance of GRS retaining walls. As global reinforcement stiffness increased, lateral facing displacements decreased and tensile forces in reinforcement increased. The same conclusion was also reached by Ling and Leshchinsky (2003) in a parametric study using finite element analysis. They concluded that toe restraint could reduce the maximum facing deformation and reinforcement strain, especially for poor quality backfill materials. For large reinforcement spacing, secondary reinforcement was effective for improving the performance of GRS walls with good quality backfill. Ling and Leshchinsky (2003) suggested that a structural facing system such as modular blocks and concrete panels could increase the stability and reduce wall deformations and reinforcement strains. This finding was later confirmed by Bathurst et al. (2006) in a series of full-scale wall tests.

Leshchinsky and Vulova (2001) investigated the effects of reinforcement spacing on failure mechanisms for GRS retaining walls using FLAC. The soil was modeled using a hyperbolic stress-strain relationship prior to failure and a Mohr-Coulomb failure criterion. The frictional connection between reinforcement and facing blocks was simulated using beam elements and interface elements. Four modes of failure were observed, including external (direct sliding and toppling), deep seated (bearing capacity), compound, and connection, based on the development of plastic zones. Deep seated failure occurred for cases with closely-spaced reinforcement and weak foundation soil. Connection failures were observed for all cases with reinforcement spacing equal to or larger than 60 cm. Leshchinsky and Vulova (2001) suggested that reinforcement spacing plays an important role in the behavior of GRS walls and significantly affects the potential failure mode.

Hatami and Bathurst (2005a; 2005b) verified their FLAC model against results from three instrumented full-scale model tests on GRS retaining walls at the end of construction. The backfill soil behavior was modeled as a nonlinear elastic-plastic material with Mohr-Coulomb failure criterion and non-associated flow rule. The hyperbolic model proposed by Duncan et al. (1980) was used to simulate nonlinear elastic stress-strain relationship of the soil prior to failure. The reinforcement was also characterized using a hyperbolic model, and was assumed to be rigidly connected to facing blocks through beam elements. In their numerical model, the effects of soil compaction during construction were simulated by applying a uniform surcharge of 8 kPa after placement of each lift. The predicted toe boundary forces, vertical foundation pressures, facing displacements, connection loads, and reinforcement strains were compared with measured results, and yielded good agreement. The influence of soil model on the wall performance was also investigated. Predicted results using a linearly-elastic perfectly-plastic soil model showed good agreement with measured wall displacements and toe boundary forces, but lesser agreement with reinforcement strain distributions. Hatami and Bathurst (2005c) and Bathurst

and Hatami (2006a) investigated the effects of different design parameters on the behavior of GRS retaining walls at the end of construction using FLAC. Results showed that, as the wall height increases, the maximum lateral displacement increases. For a granular soil, a value of cohesion as low as 10 kPa can significantly reduce lateral facing displacement and can also influence the facing deformation pattern and distribution of reinforcement strain.

Hatami and Bathurst (2006b) and Bathurst and Hatami (2006b) further validated their FLAC model for GRS retaining walls under surcharge loading using results from instrumented full-scale model tests. Bathurst et al. (2008) and Huang et al. (2010) conducted numerical simulations to investigate the influences of toe restraint conditions on the performance of GRS walls using the validated FLAC model. They found that deformation at the base of the wall and reinforcement loads increased as the toe stiffness decreased. Huang et al. (2009) also investigated the influence of soil constitutive model on the behavior of GRS retaining walls using FLAC. The soil constitutive models were linearly elastic plastic Mohr-Coulomb, modified Duncan-Chang hyperbolic, and Lade's single hardening model. Predicted results using three constitutive models were evaluated by comparing with measured results at the end of construction and under surcharge loading conditions. Huang et al. (2009) concluded that the simple Mohr-Coulomb model is better suited for studying GRS walls that are at incipient failure conditions than for working stress conditions. The Lade's model can simulate the shear dilatancy and strain softening behavior of soil during shearing; however, this model requires many parameters that lack physical meaning. On the other hand, the modified Duncan-Chang model can reasonably predict the response of GRS walls under work stress conditions, and the model parameters can be determined from conventional triaxial tests.

3.2 Dynamic Analysis of Geosynthetic-Reinforced Soil (GRS) Retaining Walls

3.2.1 Experimental Studies

3.2.1.1 Shaking Table Tests

Richardson and Lee (1975) pioneered the use of shaking table tests on reduced-scale reinforced soil walls subjected to sinusoidal motions. This study was followed by a 6.1 m high full-scale steel reinforced soil wall subjected to both forced vibrations and blast excitations (Richardson et al. 1977). Chida et al. (1982) carried out a series of shaking table tests on 4.4 m high retaining walls reinforced with steel strips. Sakaguchi (1996) compared the dynamic responses of wrapped-face geogrid reinforced soil wall with unreinforced conventional retaining walls. The reinforced wall failed at much higher acceleration than the unreinforced walls, which indicated that the GRS walls were more stable than conventional retaining wall under seismic loading. This study also concluded that light-weight rigid facing could reduce lateral facing displacements.

Koseki et al. (1998) conducted shaking table tests on 0.5 m to 0.53 m-high models of reinforced soil walls with rigid facing and conventional retaining walls. The wall models were subjected to

sinusoidal excitation at a frequency of 5 Hz and indicated a primary failure mode of overturning. They found that increasing the reinforcement length near the top of the wall could increase the resistance against overturning. Likewise, Matsuo et al. (1998) conducted shaking table tests on 1.0 m to 1.4 m high geogrid-reinforced walls to investigate the effects of reinforcement length, wall height, wall facing type, wall facing batter, and input acceleration history on dynamic response. Matsuo et al. (1998) found that increasing reinforcement length is the most effective means to reduce lateral facing displacement and that the wall with continuous rigid facing experienced larger displacements than the wall with segmental facing panels.

El-Emam and Bathurst (2004; 2005; 2007) performed a series of shaking table tests on reduced-scale reinforced soil walls with a full-height rigid facing panel to investigate the influences of toe boundary conditions, facing conditions, reinforcement layout, and input motion on dynamic response. Fourteen 1/6 scale walls with a full-height rigid facing panel were subjected to stepped-amplitude sinusoidal loading. The walls were 1 m high and the backfill soil was 2.4 m long, as shown in Figure 3.3. Excitations were applied in 0.05 g increments with a duration of 5 seconds and continued until excessive wall deformations occurred. The backfill soil had a peak friction angle of 51° and a dilation angle of 15° . Experimental results showed that facing lateral displacement could be reduced by using (1) smaller facing panel mass, (2) inclined facing panels, (3) longer reinforcement, (4) stiffer reinforcement, and (5) smaller vertical reinforcement spacing. Reinforcement load was the largest at the facing connections both at the end of construction and during shaking. The sum of reinforcement connection loads generally decreased with increasing facing mass, greater horizontal toe restraint and greater facing inclination angle. A restrained toe with a stiff facing panel was found to carry a significant portion of total horizontal earth force under both static and dynamic conditions.

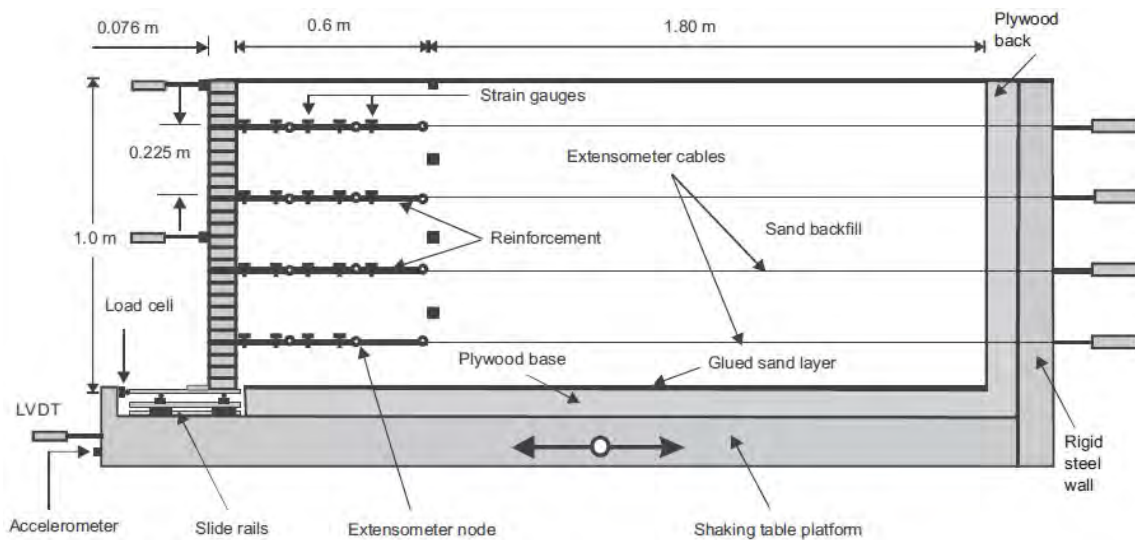


Figure 3.3. Cross-section arrangement and instrumentation layout of reduced-scale reinforced soil model walls (El-Emam and Bathurst 2005).

Ling et al. (2005a) conducted full-scale shaking table tests on three GRS walls with modular block facing for Kobe earthquake ground motion. The walls were 2.8 m high and had a 0.2 m-thick foundation soil. The layout and instrumentation for Wall 1 is shown in Figure 3.4. Walls 1 and 2 were subjected to horizontal shaking, whereas Wall 3 was subjected to both horizontal and vertical shaking. For the first excitation for each wall, the ground motion record was scaled to $PGA = 0.4 g$, and to $PGA = 0.8 g$ in the second excitation. The backfill and foundation soil was a fine sand with medium relative density and frictional angle = 38° . Experimental results showed that the GRS walls experienced negligible deformation under moderate earthquake loading ($PGA = 0.4 g$) and performed well under strong earthquake loading with $PGA = 0.8 g$. Ling et al. (2005a) found that using longer reinforcement at top layer and smaller reinforcement vertical spacing improved the seismic performance of GRS walls. Vertical acceleration did not have a large influence on wall deformation, but increased vertical stresses at foundation level and reinforcement loads. Ling et al. (2012) performed another set of shaking table tests on GRS walls constructed using a silty sand mixture with 43.3% fines content. The backfill and foundation soil had a frictional angle of 39° and apparent cohesion of 40 kPa. These walls were subjected to both horizontal and vertical Kobe earthquake motions. Comparing experimental results with previous tests results (Ling et al. 2005a), they found that GRS walls constructed using low-quality backfill soil had better seismic performance than otherwise identical walls with sandy backfill with respect to wall deformation, dynamic earth pressure and reinforcement

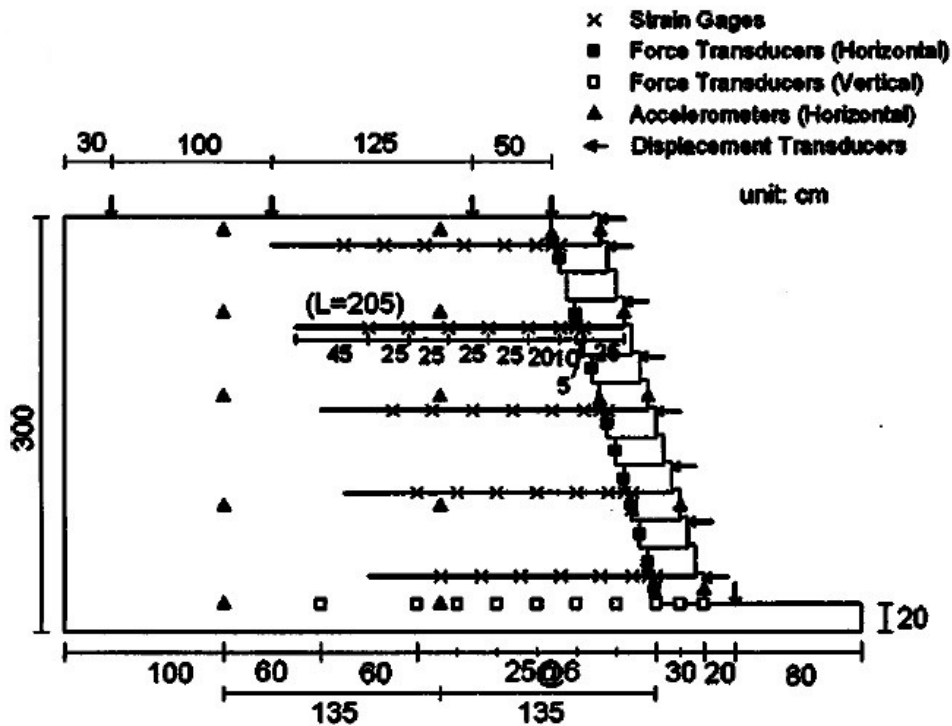


Figure 3.4. Cross-section instrumentation and layout of Wall 1 in full-scale shaking table tests (Ling et al. 2005a).

forces. Ling et al. (2012) suggested that the relatively good seismic performance was due to the apparent cohesion of the fine-grained soil. However, they cautioned against the use of apparent cohesion in the design, as such cohesion could vary significantly due to environmental changes during the service life of GRS walls.

Latha and Krishna (2008) studied the influence of backfill relative density on the seismic response of GRS walls with wrapped facing and a full-height rigid facing panel. A total of 24 walls were subjected to sinusoidal excitations on shaking table. Lateral facing displacements for walls with wrapped facing were generally much larger than walls with a full-height rigid facing panel. The effects of backfill relative density on the seismic response of GRS walls were pronounced only at low relative densities and higher base excitations. Krishna and Latha (2009) also investigated the effects of reinforcement on seismic performance of GRS walls with a full-height rigid facing. Reinforcement layers, even with low tensile strength, were very effective in reducing lateral facing displacements compared with measured displacements of unreinforced walls. However, acceleration amplification within the backfill was not much influenced by reinforcement properties.

3.2.1.2 Dynamic Centrifuge Tests

Sakaguchi (1996) conducted dynamic centrifuge tests to simulate a 4.5 m high GRS wall. Three geotextile reinforcements with different maximum tensile strength and reinforcement length were used in the tested walls. The lateral facing displacement generally decreased with increasing reinforcement length, and the optimal reinforcement length was determined to be between $2/3 H$ and H . The maximum tensile force in the geotextile was found to have little influence on seismic responses of the walls, as the tensile forces developed during seismic events were well below the respective tensile limits.

Takemura and Takahashi (2003) used centrifuge testing to study the effects of reinforcement length, vertical reinforcement spacing, and backfill dry density on the dynamic response of GRS walls. The prototype wall was 7.5 m high and subjected to sinusoidal excitation. The wall specimen with low backfill dry density experienced larger horizontal translation and larger tensile strains in the reinforcement. Ling et al. (2004) later validated their finite element model using measured data from this centrifuge test. Siddharthan et al. (2004) carried out centrifuge tests on bar mat-reinforced soil retaining walls subjected to step waves and earthquake ground motions. Test results showed that the maximum lateral facing displacement occurred at the mid-height of the reinforced walls. As expected, walls with longer reinforcement experienced less deformation.

Liu et al. (2010) conducted dynamic centrifuge tests on three GRS walls with modular block facing. The walls had a prototype height of 7.8 m. Two walls were subjected to Kobe earthquake ground motion with PGA scaled to 0.24 g, and the other was excited using a

sinusoidal wave with $PGA = 0.114$ g. Accelerations were amplified considerably in both reinforced and retained zones under modest seismic shaking. Liu et al. (2010) suggested that the design of high GRS walls may need to consider the change of acceleration with height.

3.2.2 Numerical Studies

3.2.2.1 Finite Element Method

Segrestion and Bastick (1988) validated a dynamic finite element model generated using the program SUPERFLUSH using measured results from a shaking table test on a steel strip-reinforced soil wall (Chida et al. 1985). Yogendrakumar et al. (1991) used the program TARA-3 to study the seismic response of 6 m-high retaining walls reinforced with steel strips. Yogendrakumar and Bathurst (1992) and Bachus et al. (1993) conducted dynamic finite element modeling of reinforced soil walls subjected to blast loading using the programs RESBLAST and DYNA3D, respectively. Yogendrakumar et al. (1992) studied the dynamic response of reinforced soil wall under blast loading using both equivalent linear approach and nonlinear incremental approach, and found that the nonlinear incremental approach gave better predictions when compared to measured results from a field test.

Cai and Bathurst (1995) conducted dynamic finite element analysis of GRS retaining walls with modular block facing using TARA-3. The cyclic shear behavior of backfill soil was modeled using a hyperbolic stress-strain relationship with Masing hysteretic rules during unloading and reloading. The reinforcement was modeled using a similar hysteretic model that accounted for the measured response of cyclic load-extension tests on unconfined geogrid specimens. Slip elements were used to simulate the interactions between different wall components. A scaled El-Centro earthquake record ($PGA = 0.25$ g) was applied to the base of GRS wall model. Relative displacements and shear forces between blocks were greatest at the reinforcement elevations and shear capacity was exceeded at some locations. Cai and Bathurst (1995) concluded that accurate estimation of block-block interface properties is important for seismic design of GRS walls. Furthermore, predicted tensile forces in the reinforcement were smaller than those calculated using the pseudo-static approach, which implies that the pseudo-static approach is conservative for seismic design and analysis of GRS walls with modular block facing.

Helwany et al. (2001) verified a finite element model generated using the program DYNA3D using measured results from a small-scale shaking table test on a 0.9 m high GRS segmental wall. Nonlinear hysteretic behavior of the backfill soil under cyclic loading was simulated using the Ramberg-Osgood model with parameters determined from laboratory tests. The geotextile was modeled as a linearly elastic material. Helwany and McCallen (2001) investigated the influence of facing block connection on the static and dynamic behavior of GRS walls with the validated model. At the end of construction, the wall using facing blocks with pin connections had smaller lateral facing displacement than the wall without pin connections, while the wall using facing blocks with pin connections experienced larger seismic-induced displacements.

Helwany and McCallen (2001) suggested that smaller seismic-induced lateral displacements in the wall without pin connections were due to smaller lateral earth pressures behind the facing, as the blocks without pin connections permit more relative sliding between blocks.

Ling et al. (2004) validated a finite element model for both static and dynamic analyses using a modified version of Diana-Swandyne II. A generalized plasticity model which accounts for stress-dependent stiffness, strength and dilatancy, as well as cyclic hardening behavior, was used to characterize the backfill soil. A bounding surface model was used to simulate cyclic behavior of uniaxial geogrid. The interactions between different components were included using interface elements. The dynamic finite element model was validated using measured results from dynamic centrifuge tests. In these tests, the GRS walls were subjected to 20 cycles of sinusoidal excitation with a frequency of 2 Hz and acceleration amplitude of 0.2 g. Predicted accelerations, wall facing displacements, crest settlement and maximum tensile forces in the geogrid were compared with measured results, and showed good agreement. Ling et al. (2005b) conducted a series of parametric studies using the validated finite element model to investigate effects of soil and reinforcement properties, reinforcement length and spacing, and block interaction properties on the performance of GRS walls at the end of construction and under earthquake loading. Lateral facing displacements and crest settlement were mainly influenced by soil cyclic behavior, reinforcement layout, and earthquake motions. The effects of reinforcement vertical spacing on wall deformation, reinforcement forces, and lateral earth pressure were more significant than reinforcement length.

Validated numerical models can be used to better understand the dynamic behavior of GRS walls. However, previous model validations have been based on either reduced-scale shaking table tests or dynamic centrifuge tests, both of which have disadvantages such as model size effects, stress level effects, and boundary condition effects. The full-scale shaking table tests on GRS walls with modular block facing (2.8 m high) conducted by Ling et al. (2005a) have provided data that can be used to calibrate dynamic numerical models. Ling et al. (2010) validated a dynamic finite element model using experimental results and improved soil and geosynthetic models based on their previous constitutive models (Ling 2003; Ling et al. 2005b). The unified general plasticity model for soil was improved by considering the effect of soil density, and the S-shaped load-strain relationship was accounted for in simulating the cyclic behavior of geogrid. Lee et al. (2010) also simulated full-scale shaking table tests using the finite element program LS-DYNA. The backfill soil was characterized using a geological cap model and the geogrid reinforcement was characterized using a plastic-kinematic model with a bilinear stress-strain curve. Lee and Chang (2012) conducted a series of parametric studies with their validated program to evaluate the effects of different design parameters, including wall height, wall batter angle, soil friction angle, reinforcement spacing, and reinforcement stiffness, on the seismic performance of GRS walls. The results showed that GRS walls become less stable with a decreasing batter angle (e.g., more near vertical) for the wall facing and a small

vertical reinforcement spacing of 0.2 m is effective in decreasing wall deformations and reinforcement forces.

3.2.2.2 Finite Difference Method

Bathurst and Hatami (1998; 1999) used FLAC to investigate the effect of different design parameters on the dynamic response of GRS walls with a rigid full-height facing panel. The dynamic response of GRS walls was most sensitive to toe boundary condition (i.e., fixed toe vs. sliding toe). Both the total lateral facing displacement at the top and the relative displacement with respect to the toe were smaller for a wall with a sliding toe condition than a wall with a fixed toe. Wall deformation decreased with increasing reinforcement stiffness and reinforcement length, but the effect was relatively small for a ratio of reinforcement length to wall height (L/H) larger than 0.7. Hatami and Bathurst (2000a) studied the effect of different structural design parameters on the fundamental frequency of GRS walls and concluded that fundamental frequency can be estimated with reasonable accuracy using a one-dimensional solution based on linear elastic theory. The results also showed that fundamental frequency was not significantly influenced by reinforcement stiffness, reinforcement length, toe restraint conditions and soil friction angle, but was dependent on ground motion intensity and the width-to-height ratio (W/H) of the backfill.

Hatami and Bathurst (2000b) simulated the dynamic response of GRS walls with modular block facing subjected to different ground motions. Deformations and reinforcement forces for GRS walls subjected to a single frequency harmonic motion were larger than the responses of walls subjected to actual earthquake ground motions with comparable predominant frequencies. They also found that low-frequency ground motions with high intensity could result in significant structural responses of short-period GRS walls. El-Emam et al. (2004) and Fakharian and Attar (2007) validated their FLAC models using measured results from reduced-scale shaking table tests on GRS walls conducted at RMC (El-Emam and Bathurst 2004; 2005). However, these validations are restricted to GRS walls with a rigid full-height facing panel.

3.3 Static Analysis of Geosynthetic-Reinforced Soil (GRS) Bridge Abutments

3.3.1 Experimental Studies

3.3.1.1 Field Project Instrumentation and Monitoring

The Colorado Department of Transportation (CDOT) completed the new Founders/Meadows Bridge project near Denver, Colorado, in 1999. In this project, geosynthetic-reinforced soil retaining walls were used to support both the bridge superstructures and approach roadways. The GRS bridge abutment system was well instrumented and monitored to assess its performance during construction stages and after opening to traffic.

Figure 3.5 shows the plan view of the two-span bridge and approach roadway structures. Each span of the bridge is 34.5 m long and 34.5 m wide, with 20 side-by-side prestressed box girders.

Section 200, Section 400 and Section 800 were instrumented to monitor behavior of the structure during and after construction. The cross-section of the GRS bridge abutment system is shown in Figure 3.6. The bridge superstructure load was transmitted through concrete abutment wall to a spread footing placed directly on the top of a GRS retaining wall. The GRS structure was reinforced using geogrid with a vertical spacing of 0.4 m. Geogrid length was 8 m at the bottom and increased linearly upward with 1V:1H slope. The backfill was a mixture of gravel, sand, and fine-grained soil, with a unit weight of 22.1 kN/m^3 . A friction angle of 39.5° and cohesion of 69.8 kPa were determined from large-scale triaxial tests.

Field monitoring was conducted to assess performance of the structure during lower wall construction, placement of bridge superstructures, and after opening to traffic. Measured movements of the structure during construction were small. At Section 800, the maximum outward displacement of the lower GRS wall facing was 12 mm at the end of lower wall construction and 10 mm due to placement of the bridge. The settlement of bridge abutment footing induced by the bridge load was 12 mm, which corresponds to 0.2% of the height of the lower GRS wall. The GRS bridge abutment system also showed very good in-service performance. After opening to traffic for 12 months, the maximum outward displacement of lower GRS wall and settlement of bridge footing were 5 mm and 10 mm, respectively. Differential settlement between the bridge abutment and approach roadway was also negligible.

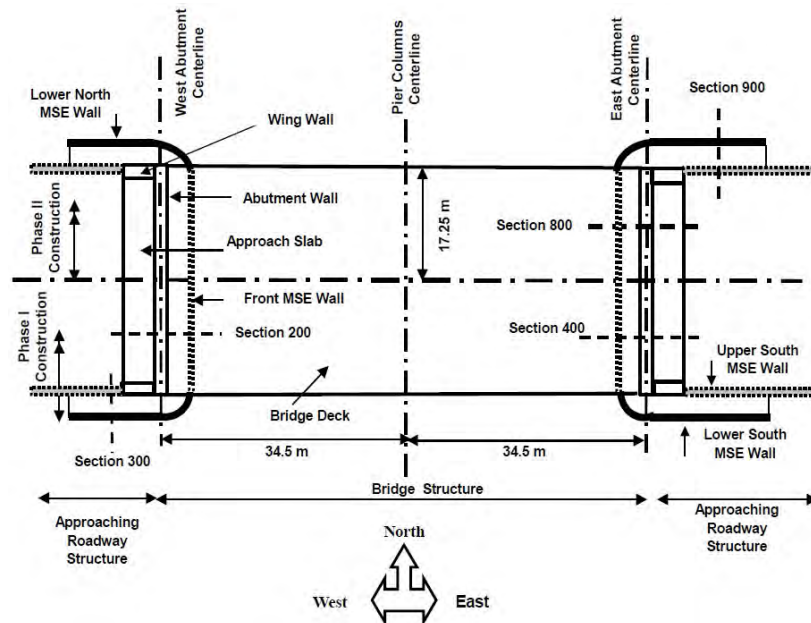


Figure 3.5. Plan view of the Founders/Meadows Bridge (Abu-Hejleh et al. 2000).

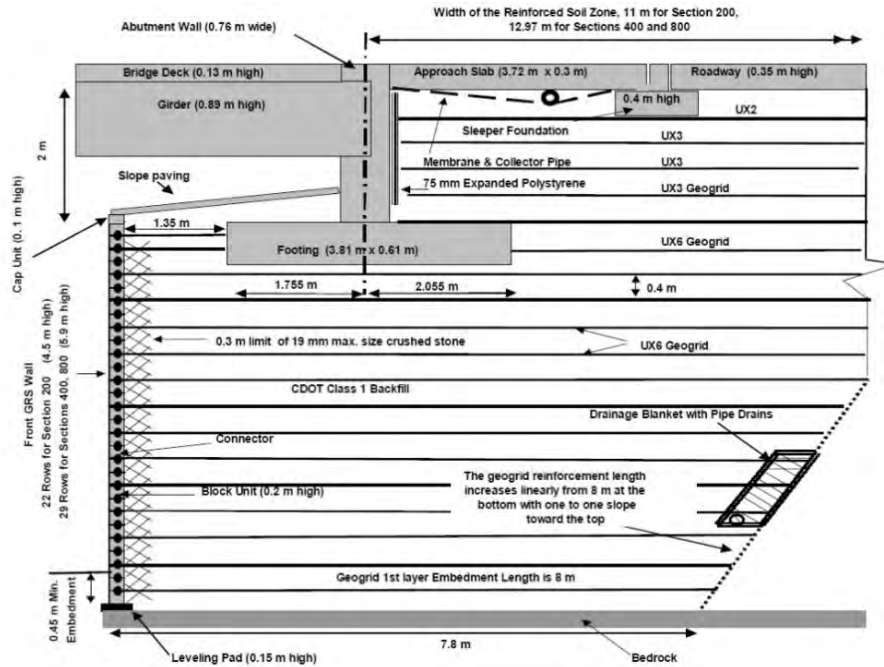


Figure 3.6. Cross-section of the GRS bridge abutment system (Abu-Hejleh et al. 2001).

3.3.1.2 Field Loading Tests

In the GRS bridge abutment system, the lower GRS walls are typically subjected to much larger loads than conventional GRS walls. Therefore, the allowable bearing pressure of a GRS bridge abutment is a major issue for design. FHWA design guidelines (Berg et al. 2009) suggest a maximum allowable bearing pressure of 200 kPa for GRS bridge abutments. Many experimental studies, usually field loading tests on full-scale structures, have been conducted to investigate the load-bearing capacity of GRS bridge piers and abutments (Gotteland et al. 1997; Adams 1997; Ketchart and Wu 1997; Wu et al. 2001).

Gotteland et al. (1997) conducted full-scale loading tests to study the failure behavior of GRS walls as bridge support structures. An embankment, referred to as the Garden Experimental Embankment, consisted of two GRS wall sections (NW wall and W wall) and was constructed for loading tests as shown in Figure 3.7. The NW wall was reinforced with a nonwoven geotextile while the W wall was reinforced with a knitted woven geotextile. The intermediate reinforcement in W wall was shorter than in NW wall. Loading was applied on top of each GRS wall through a foundation slab. The applied loads at failure were 140 kN/m with a settlement of 36 mm and 123 kN/m with a settlement of 33 mm for the NW wall and W wall, respectively.

Figure 3.8 shows the cross-section of a 5.4 m high full-scale bridge pier tested at the Turner-Fairbank Highway Research Center in McLean, Virginia (Adams 1997). The GRS pier was reinforced with woven polypropylene geotextile at a vertical spacing of 0.2 m. The pier at the

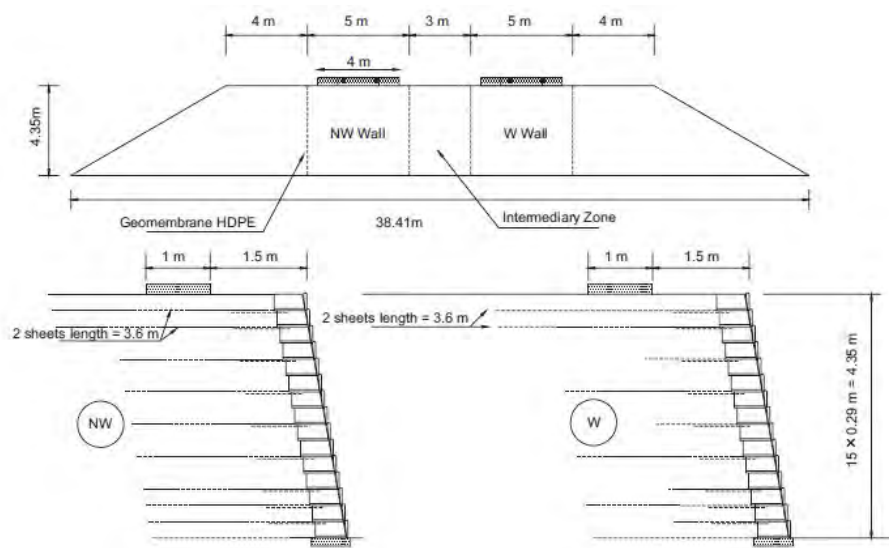


Figure 3.7. The Garden Experimental Embankment (Gotteland et al. 1997).

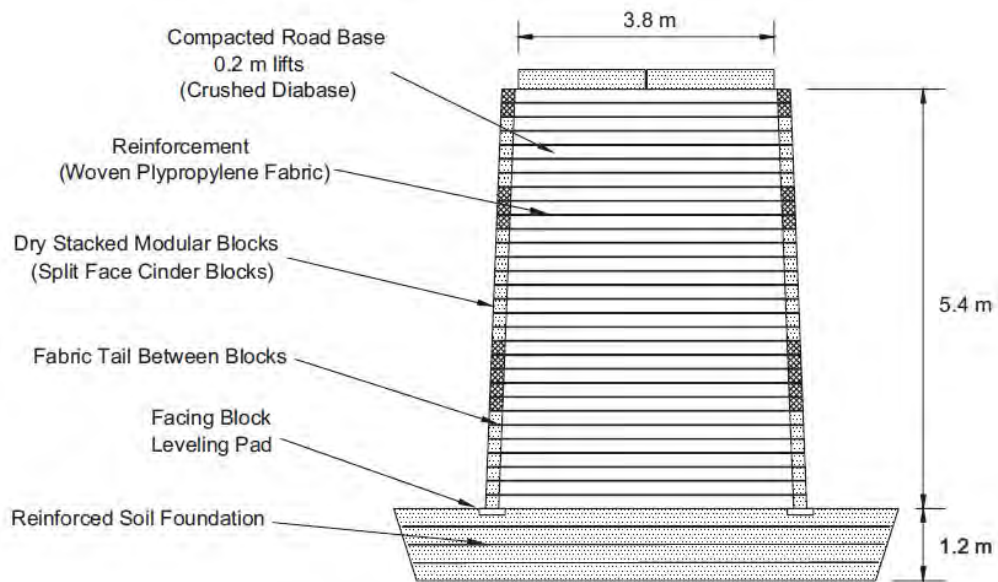


Figure 3.8. Cross-section of the FHWA Turner-Fairbank GRS bridge pier (Adams 1997).

intermediate height of 3.0 m was loaded to 200 kPa and responded with a settlement of 13 mm and a maximum lateral facing displacement of 6 mm. This was considered satisfactory performance. At full height, the pier was loaded to failure at a vertical pressure of 900 kPa with a settlement of approximately 70 mm.

Ketchart and Wu (1997) conducted full-scale load tests on two bridge piers and one abutment, called the Havana Yard GRS bridge piers and abutment. The outer pier and abutment were 7.6 m high and the center pier was 7.3 m high, as shown in Figure 3.9. Each structure was reinforced with geotextile at a vertical spacing of 0.2 m. In the loading tests, steel girders and concrete blocks were used to simulate the bridge superstructure load and applied vertical pressures of 232 kPa and 130 kPa on the outer pier and abutment, respectively. Measured settlements under the applied loads were 36.6 mm in the pier and 27.1 mm in the abutment. The settlement in the pier was larger than that in the abutment because the pier was subjected to a larger stress.

Two GRS bridge abutments were constructed in Black Hawk, Colorado, to support a 36 m span steel arch bridge (Wu et al. 2001). In each abutment, two square footings were placed on top of the lower wall and one strip footing was constructed on the upper wall as shown in Figure 3.10. The abutments were reinforced with woven geotextile at a vertical spacing of 0.3 m. Four square footings were preloaded using a vertical pressure of 245 kPa, and then reloaded to the design load of 150 kPa. Results indicated that settlements of four square footings at the design load could be reduced by a factor of 1.5 to 6 by the preloading process (245 kPa).

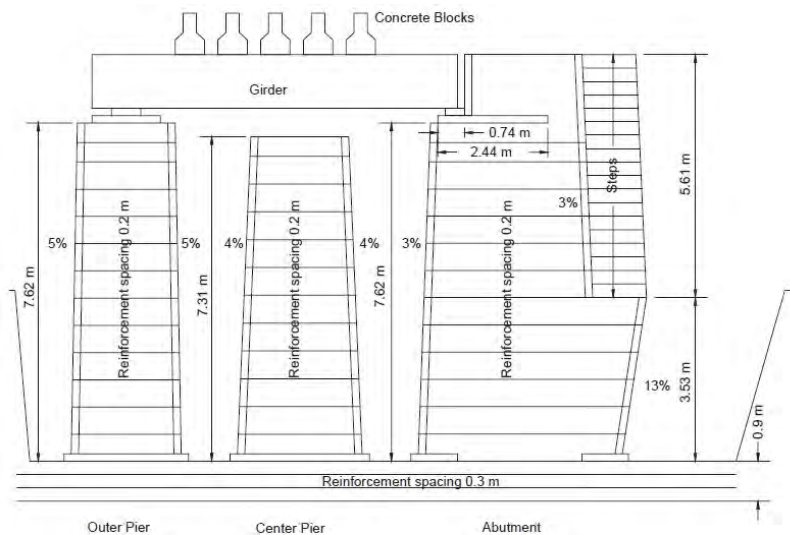


Figure 3.9. Cross-section of the Havana Yard GRS bridge pier and abutment (Ketchart and Wu 1997).

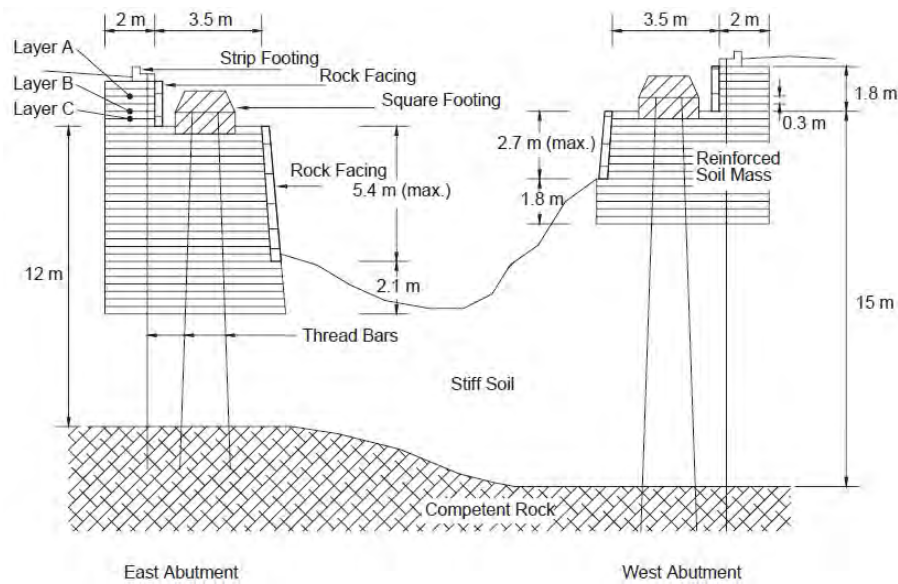


Figure 3.10. Cross-section of the Black Hawk bridge abutments (Wu et al. 2001).

3.3.2 Numerical Studies

Numerical modeling has been used to study the static behavior of GRS bridge abutments. Skinner and Rowe (2005) conducted finite element analyses to study the behavior of GRS bridge abutment constructed on a yielding clay foundation. Zevgolis and Bourdeau (2007) also studied the deformation behavior of GRS bridge abutments with different foundation soil conditions using the program PLAXIS. Some numerical models have been verified against results from field monitoring and/or field loading tests, which could provide more convincing insights on the behavior of GRS bridge abutments (Helwany et al. 2003; Wu et al. 2006a; Helwany et al. 2007; Fakharian and Attar 2007).

Helwany et al. (2003) performed finite element analyses using the program DACSAR. The model was verified by comparing results with measurements for the Founders/Meadows GRS bridge abutment. The soil was simulated as a nonlinear elastic material using the Duncan-Chang model and interfaces between concrete blocks, between blocks and reinforcement, and between blocks and backfill soil were included. The geosynthetic reinforcement was assumed to be linearly elastic and perfectly bonded to backfill soils. Helwany et al. (2003) also investigated the effects of foundation soil condition on behavior of the GRS bridge abutment. Results showed that a loose sand foundation can produce much larger settlements and lateral facing displacements than a dense sand foundation. For all sand and clay foundation soil conditions, differential settlements between the bridge abutment and approach roadway were acceptable.

Wu et al. (2006b) conducted a series of finite element analyses using DYNA3D/LS-DYNA to investigate the effects of bridge seat type, seat width, soil stiffness/strength, reinforcement spacing, and foundation stiffness on the load-bearing capacity of GRS bridge abutments. Maximum allowable bearing pressures for the abutments were determined based on a limiting displacement criterion or a limiting shear strain criterion. Results indicated that reinforcement spacing is the most important factor that influences the load-bearing capacity of a GRS bridge abutment. In that study, abutments with a reinforcement spacing of 0.2 m could sustain a vertical pressure up to 1000 kPa without facing failure. Based on simulation results, a table was developed to determine the recommended design bearing pressure for different abutment configurations and soil conditions.

Helwany et al. (2007) carried out finite element analyses using DYNA3D to simulate two full-scale load tests on GRS bridge abutments. The soil behavior was simulated using a cap plasticity model and the geosynthetic reinforcement was modeled using an elastic-plastic model. The numerical analyses investigated the performance of GRS bridge abutments under service load and failure load conditions. Parametric studies were also conducted to investigate the behavior of GRS bridge abutments under live and dead loads from bridge superstructures. Results indicated that soil friction angle, reinforcement spacing, and reinforcement stiffness are important factors that influence the behavior of GRS bridge abutments.

3.4 Dynamic Analysis of Geosynthetic-Reinforced Soil (GRS) Bridge Abutments

3.4.1 Experimental Studies

Helwany et al. (2012) conducted large-scale shaking table tests on a GRS bridge abutment at the U.S. Army Engineering Research and Development Center – Construction Engineering Research Laboratory (ERDC-CERL) using the Triaxial Earthquake and Shock Simulator (TESS). Figure 3.11 shows the configuration of the test specimen. The total height of the abutment was 3.6 m and the lower wall was 3.2 m high. The abutment soil was reinforced with a woven geotextile at a vertical spacing of 0.2 m. The soil had an optimum moisture content of 6.8% and a unit weight of 21.5 kN/m³. The friction angle of the reinforced and retained soils was 44°. The total load from bridge superstructure was 445 kN.

In the shaking table tests, the GRS bridge abutment model was tested using a staged sinusoidal horizontal motion with increasing amplitude in the longitudinal direction. The first test was performed using sinusoidal motion at a frequency of 1.5 Hz with an amplitude of 0.15 g for 20 seconds. Four additional tests were conducted at a frequency of 3 Hz with amplitudes of 0.3 g, 0.45 g, 0.67 g, and 1.0 g. The GRS bridge abutment model performed well with small lateral facing displacements and seat settlements during the first sinusoidal motion test. In general, the GRS bridge abutment remained functional under sinusoidal motions with amplitudes up to 1.0 g.

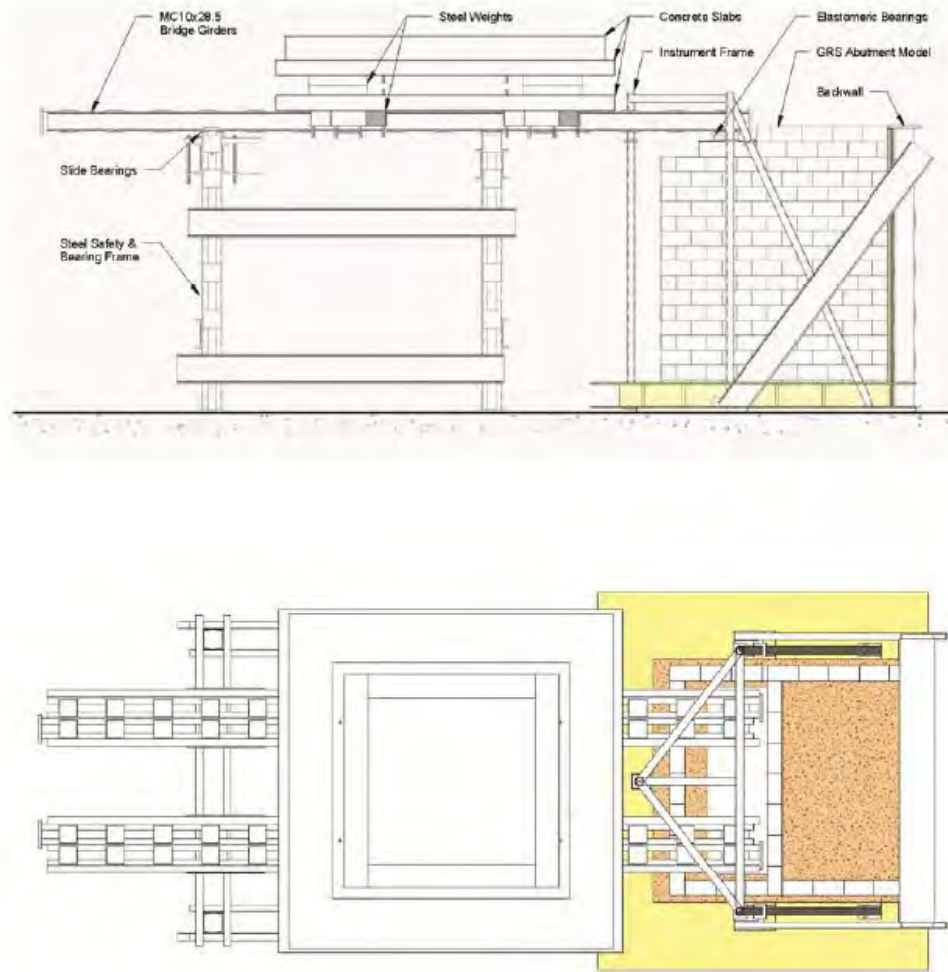


Figure 3.11. Configuration of large-scale shaking table test of GRS bridge abutment (Helwany et al. 2012).

3.4.2 Numerical Studies

Helwany et al. (2012) validated a 3-D ABAQUS finite element model with measured results from the results of the full-scale shaking table tests on the GRS bridge abutment. The backfill soil was simulated using a cyclic model with isotropic/kinematic hardening and the geotextile was modeled using membrane elements. Interface elements that allow sliding and separation were also placed between blocks and reinforcement, between soil and reinforcement, and between blocks and soil. Parametric studies were conducted to investigate the influences of various factors, including friction angle of soil, reinforcement stiffness, reinforcement spacing, bridge height, bridge span, and earthquake ground motion, on the seismic performance of GRS bridge abutments. The simulation results indicated that GRS bridge abutments would generally experience small seat settlements (less than 5 cm) and relatively large facing lateral displacements (up to 20 cm) for strong earthquake motions.

Chapter 4 – Research Tasks

The objective for Phase I of the project was to perform analytical/numerical studies leading up to a proposal to perform large-scale shake table tests of geosynthetic-reinforced soil (GRS) abutments for longitudinal and transverse loading conditions. Numerical modeling studies were conducted primarily using FLAC-2D version 7.0 (Itasca 2011), which has a long track record of success for analysis of GRS structures (Bathurst and Hatami 1998; Hatami and Bathurst 2000; Zarnani and Bathurst 2009; Huang et al. 2010). Investigations were conducted for GRS structures with and without bridge loads for both static and seismic loading conditions. Investigated variables included geometry, reinforcement type and layout, backfill soil properties, magnitude of bridge load, and earthquake ground motion record. Results of FLAC analyses were also compared to field measurements for static loading, dynamic loading of a large-scale GRS wall, and results obtained using ABAQUS to provide additional validation.

The work for Phase I was divided into the following tasks:

Validation of FLAC for static analysis of GRS bridge abutment – FLAC modeling results were compared with field measurements for static loading of the Founders/Meadows GRS bridge abutment in Colorado.

Numerical simulations of GRS retaining wall for seismic loading – Results of FLAC simulations were compared with measurements for a full-scale test of a GRS retaining wall on the UCSD outdoor shake table.

Numerical simulations of seismic response of GRS abutments in the longitudinal direction – FLAC was used to simulate the seismic response of a 150 ft. bridge with GRS abutments and shaking in the longitudinal direction.

Comparison of FLAC and ABAQUS results for seismic response of GRS bridge abutments in the longitudinal direction – Results of FLAC and ABAQUS simulations were compared for a 150 ft. bridge with GRS abutments and shaking in the longitudinal direction.

Numerical simulations of seismic response of GRS abutments in the transverse direction – FLAC was used to simulate the seismic response of a 150 ft. bridge with GRS abutments and shaking in the transverse direction.

Results for each of these research tasks are presented in Chapters 5 - 9. Conclusions are presented in Chapter 10.

Chapter 5 – Validation of FLAC for Static Analysis of GRS Bridge Abutment

5.1 Description of the Founders/Meadows GRS Bridge Abutment

The Founders/Meadows GRS bridge project was completed by the Colorado Department of Transportation (CDOT) in 1999 and includes GRS walls to support the bridge and approach roadways. Figure 5.1 shows a typical cross-section. The bridge abutment consisted of a 6 m high lower GRS wall and a 2 m high upper GRS wall. Bridge loads were transmitted to the top of lower wall through a spread footing. The footing had a width of 3.81 m and is offset 1.35 m from the back of the lower wall. The GRS bridge abutment was constructed in six stages as indicated in Figure 5.1. The backfill soil was specified as CDOT Class 1 structural backfill, and consisted of a mixture of gravel (35%), sand (54.4%), and fines (10.6%). The geogrid was Tensar UX 6 for the lower wall and Tensar UX 3 and UX 2 for the upper wall. Geogrid length was 8 m at the bottom and increased linearly upward with 1V:1H slope. Geogrid layers were placed with a vertical spacing of 0.4 m. The dimensions of concrete modular block facing elements were 0.28 m (width) × 0.2 m (height). The abutment was fully instrumented and monitored during construction and after opening to traffic. The instrumented Section 800 is shown in Figure 5.2. A detailed description of this project is presented by Abu-Hejleh et al. (2000).

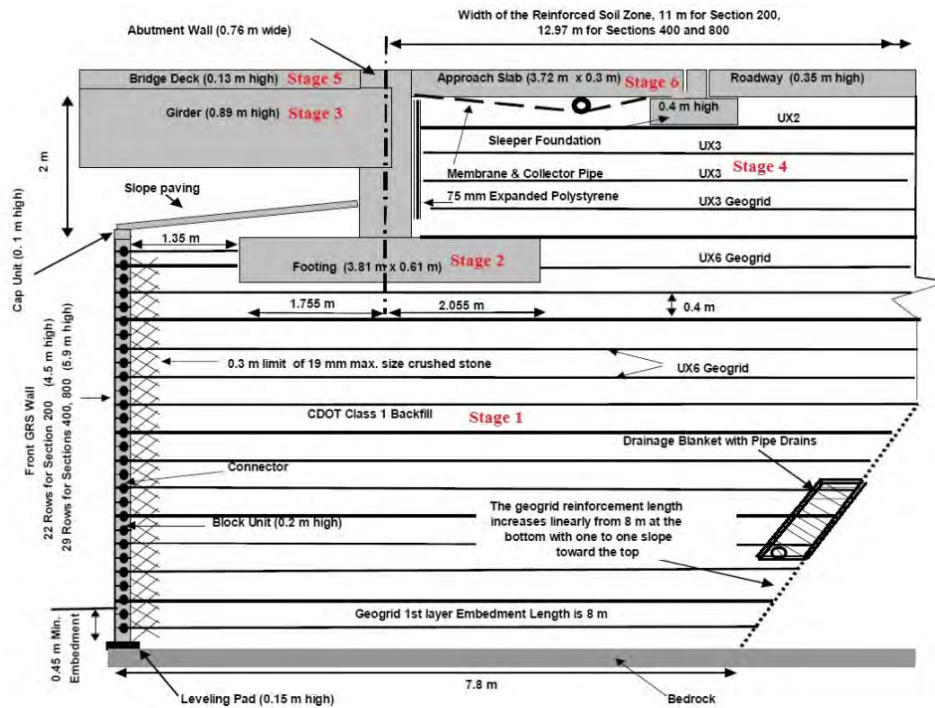


Figure 5.1. Typical cross-section of Founders/Meadows GRS bridge abutment showing geometry and construction stages (Abu-Hejleh et al. 2000).

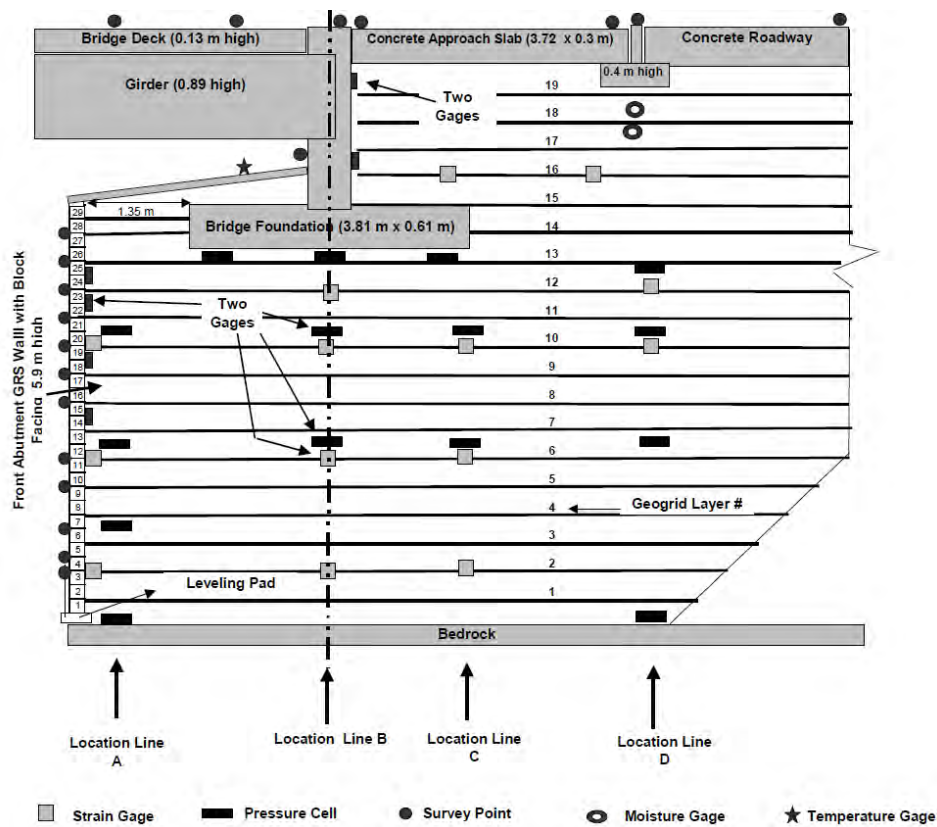


Figure 5.2. Layout of instrumented Section 800 for the Founders/Meadows GRS bridge abutment (Abu-Hejleh et al. 2000).

5.2 Numerical Model

FLAC-2D was used to simulate the static response of the Founders/Meadows GRS bridge abutment, including the construction sequence. The in-service performance after opening to traffic was simulated by applying a surcharge load on the top surface of bridge deck and approach roadway.

5.2.1 Finite Difference Grid and Boundary Conditions

The finite difference grid for the abutment model is shown in Figure 5.3. The foundation soil was 6 m deep below the GRS bridge abutment structure. The lateral boundary for the FLAC model was located at a distance of 32 m ($4H$) behind the lower wall facing to minimize the influence of boundary conditions on the results. The lateral boundary for the model was fixed in the horizontal direction and free to move in the vertical direction, whereas the bottom boundary was fixed in both horizontal and vertical directions.

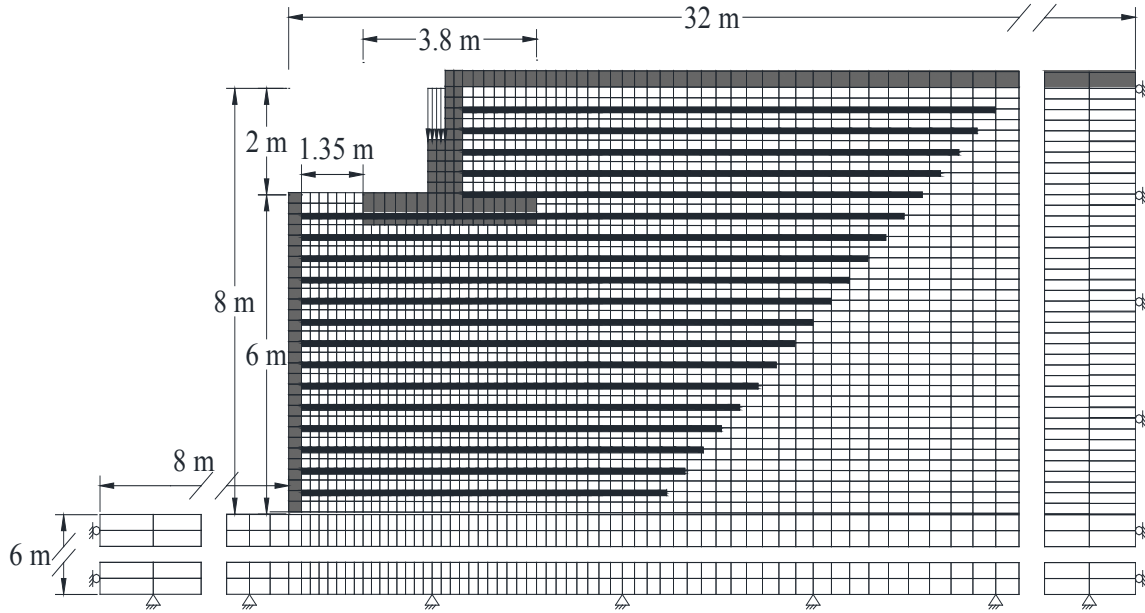


Figure 5.3. FLAC finite difference grid for the Founders/Meadows GRS bridge abutment.

5.2.2 Material Models and Properties

The concrete facing blocks and bridge seat were modeled as elastic materials with modulus $E = 20$ GPa and Poisson's ratio $\nu = 0.2$. A very stiff foundation soil was used in the simulations. The backfill soil was modeled as an elastoplastic dilatant material with a Mohr-Coulomb failure criterion and a non-associated flow rule. The Duncan-Chang hyperbolic relationship (Duncan et al. 1980) was used to simulate non-linear stress-strain behavior of backfill soil prior to failure. Backfill soil parameters were calibrated with measured results from large-scale triaxial tests. Parameters for the backfill soil are summarized in Table 5.1. In Figure 5.4, a comparison between predicted and measured results from the triaxial tests shows generally good agreement, except for volumetric strains under low stress. Geogrid reinforcement was simulated using cable elements with a tensile stiffness of 2000 kN/m in the lower wall and 1000 kN/m in the upper wall. Soil-geogrid interfaces were characterized using $c = 0$ and $\phi = 39.5^\circ$ and allow for interface sliding. The soil-block, block-block, and soil-bridge footing interfaces were modeled using interface elements with $c = 0$ and friction angles equal to 26° , 35° , and 26° , respectively.

Table 5.1. Model parameters for backfill soil for the Founders/Meadows GRS bridge abutment.

| Unit weight γ (kN/m ³) | Elastic modulus K | Elastic modulus exponent n | Failure ratio R_f | Bulk modulus K_b | Bulk modulus exponent m | Atmospheric pressure p_a (kPa) | Cohesion c' (kPa) | Friction angle ϕ' ($^\circ$) | Dilation angle ψ ($^\circ$) |
|---|---------------------|------------------------------|---------------------|--------------------|---------------------------|----------------------------------|---------------------|-------------------------------------|------------------------------------|
| 22.1 | 1000 | 0.6 | 0.72 | 800 | 0 | 100 | 69.8 | 39.5 | 6 |

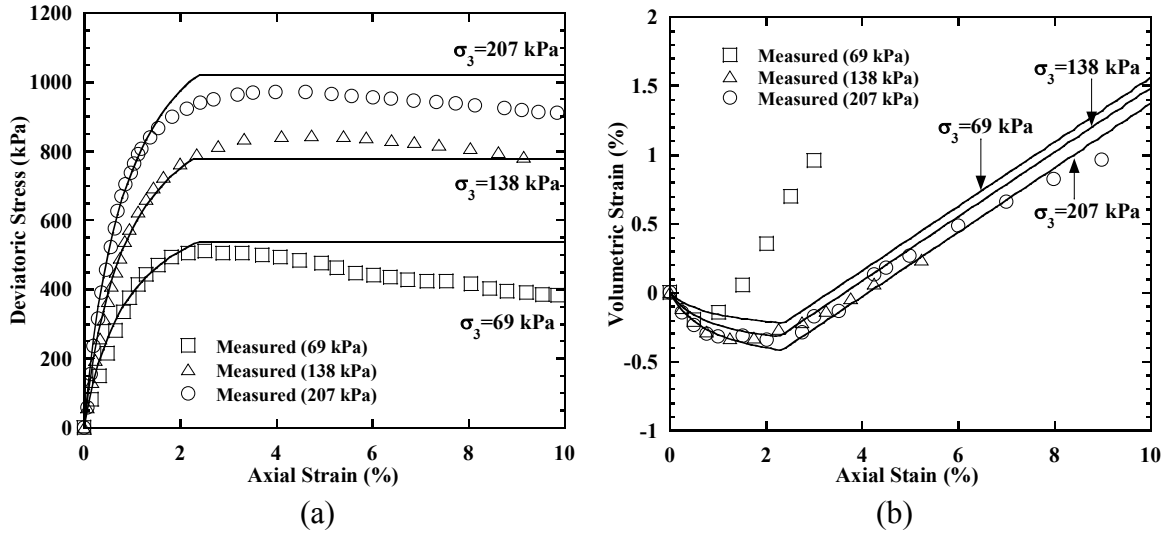


Figure 5.4. Comparison of measured and predicted results from triaxial tests: (a) deviatoric stress vs. axial strain; (b) volumetric strain vs. axial strain.

5.3 Simulation Results

Numerical results for the Founders/Meadows GRS bridge abutment, including wall lateral facing displacements, bridge footing settlement, geogrid strains, lateral earth pressures and vertical stresses during different construction stages are presented and compared with measured results (Section 800, Figure 5.2) in the following sections. Measured data were extracted from the report by Abu-Hejleh et al. (2001).

5.3.1 Key Deformations of GRS Bridge Abutment

Table 5.2. Summary of measured and predicted incremental displacements for Founders/Meadows GRS bridge abutment.

| | After Lower Wall Construction (Stage 1) | Due to Placement of Bridge (Stages 2-6) | Due to Traffic Loading (Stage 7) |
|---|---|---|----------------------------------|
| Incremental Maximum Lateral Facing Displacement (mm) | | | |
| Measured | 12 | 10 | 5 |
| Predicted | 11 | 12 | 5 |
| Incremental Settlement of Bottom GRS Wall Facing Block (mm) | | | |
| Measured | 8 | 3 | 3 |
| Predicted | 5 | 4 | 1 |
| Incremental Settlement of Bridge Footing (mm) | | | |
| Measured | - | 12 | 10 |
| Predicted | - | 12 | 5 |

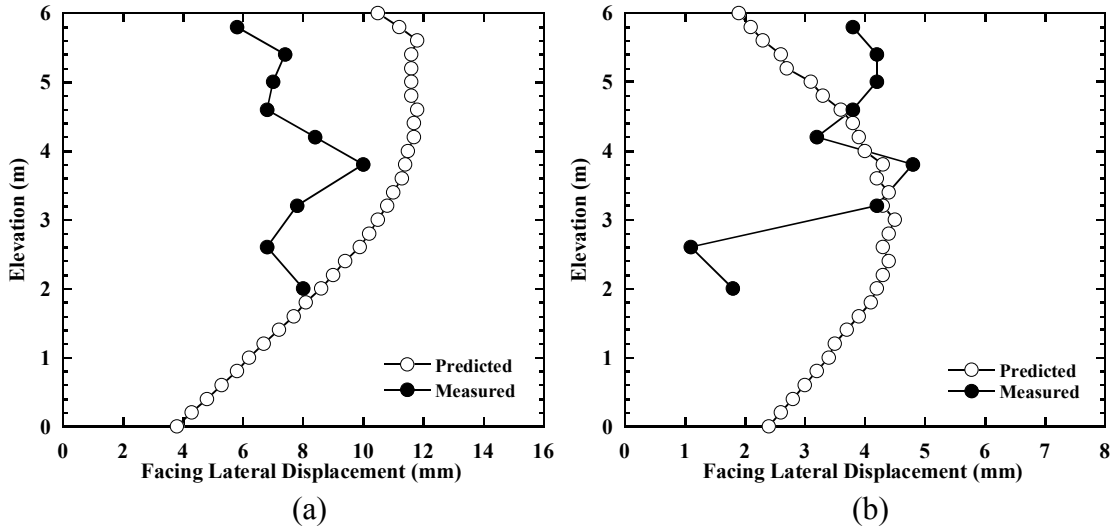


Figure 5.5. Incremental lateral facing displacements: (a) at end of construction; (b) due to traffic loads.

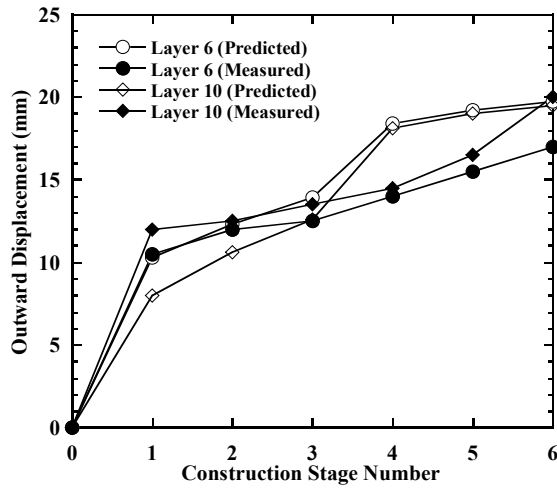


Figure 5.6. Outward displacements at elevations of geogrid layers 6 and 10 [see Figure 5.1 for construction stages].

5.3.2 Geogrid Strains

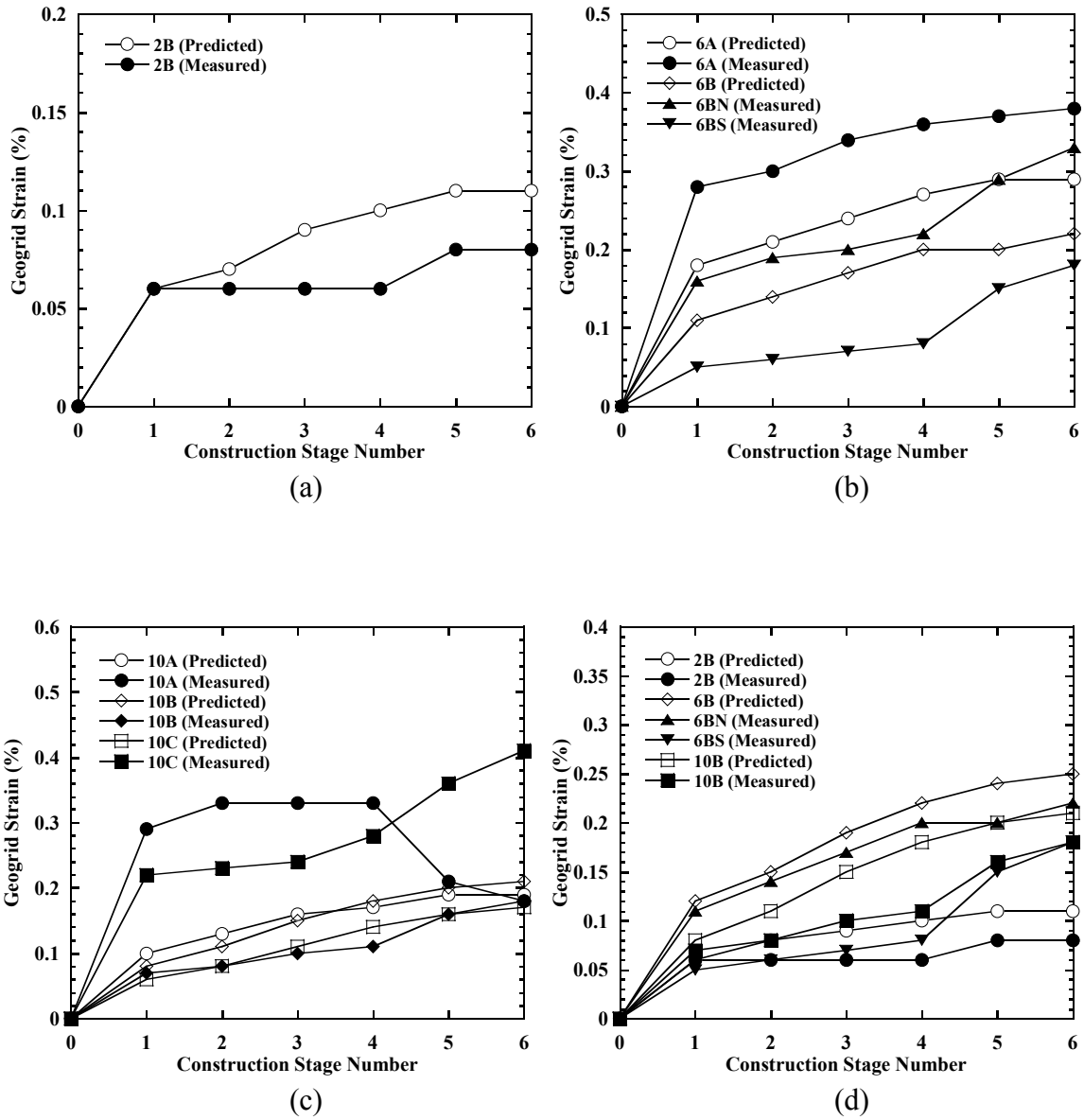


Figure 5.7. Geogrid strains at: (a) Layer 2; (b) Layer 6; (c) Layer 10; (d) Line B. [notation: 10A indicates geogrid layer 10, vertical line A, in Figure 5.2]

5.3.3 Lateral Earth Pressures

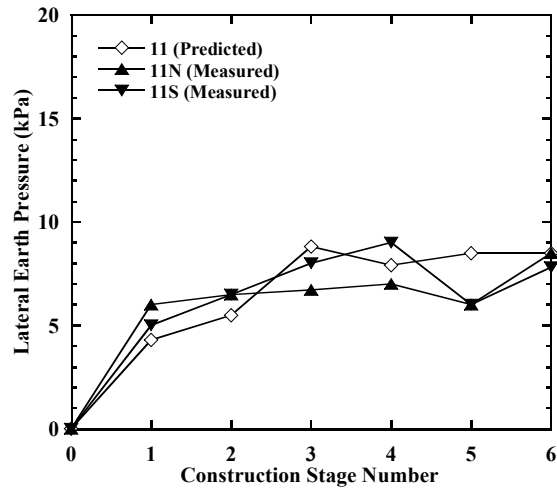


Figure 5.8. Lateral earth pressures behind lower wall facing at elevation of 4.5 m.

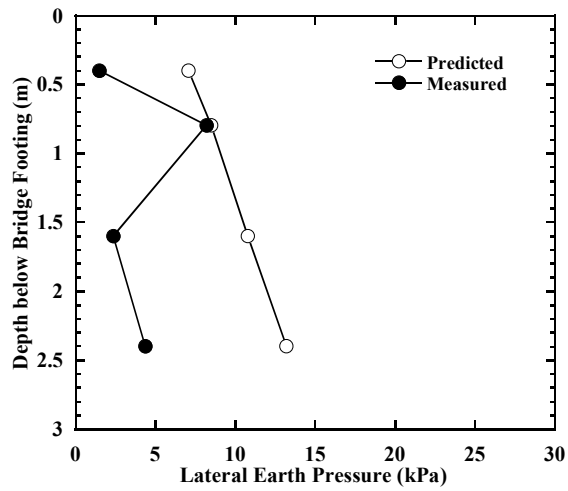


Figure 5.9. Lateral earth pressures behind lower wall facing at the end of construction.

5.3.4 Vertical Stresses

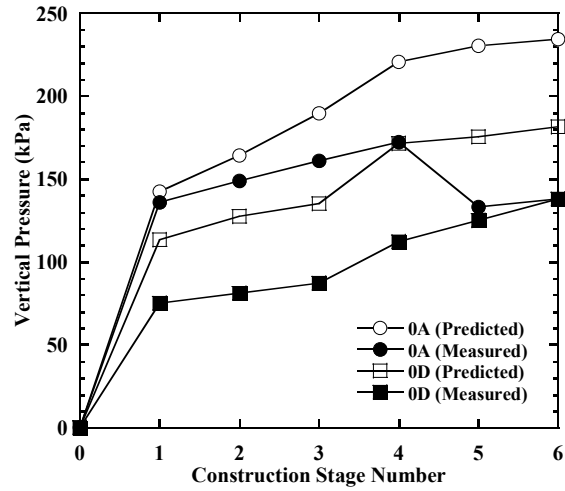


Figure 5.10. Vertical stresses at the base of bridge abutment.

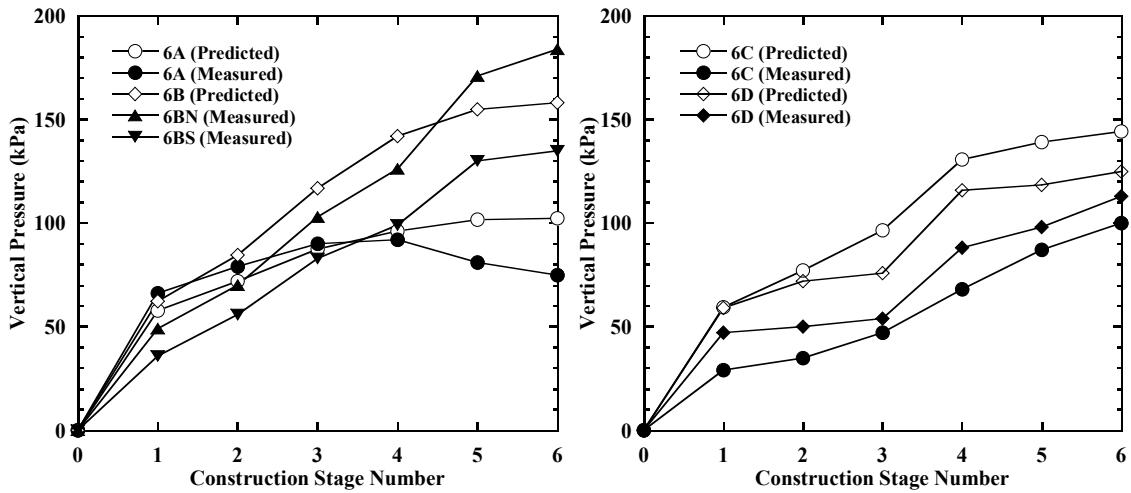


Figure 5.11. Vertical stresses at elevation of 2.3 m from top of bedrock.

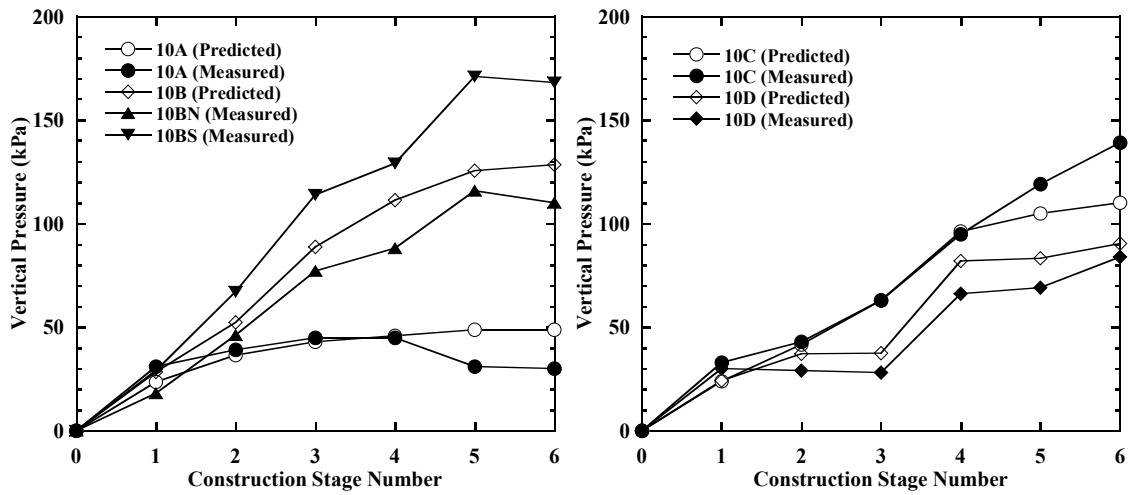


Figure 5.12. Vertical stresses at elevation of 4.1 m from top of bedrock.

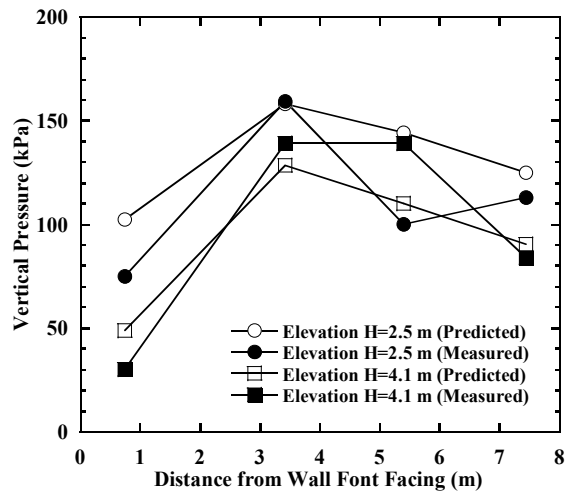


Figure 5.13. Vertical stresses at the end of construction.

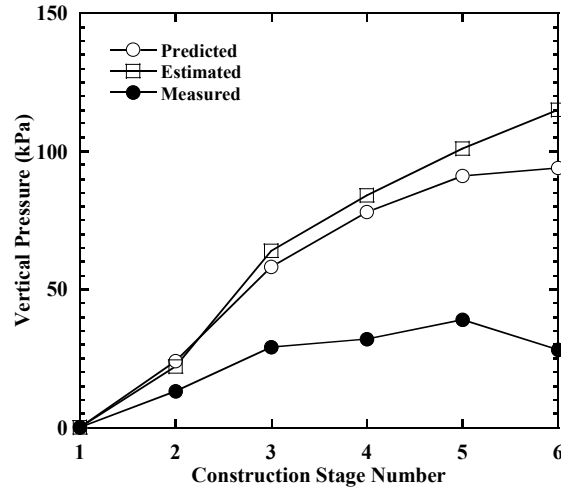


Figure 5.14. Vertical stresses under bridge footing at different construction stages.

5.4 Summary

The results presented in this chapter indicate that: (1) static loading displacements of the GRS bridge abutment for both end-of-construction and in-service conditions were small, and (2) FLAC did a good job in predicting these displacements. Table 5.2 shows that measured and predicted maximum lateral displacements after construction for the lower GRS wall were 12 mm and 11 mm, respectively. Measured and predicted settlements of the bridge footing due to placement of the bridge were both 12 mm, which corresponds to 0.2% of the lower wall height. Figure 5.5(a) shows the measured and predicted lateral displacement profiles due to placement of bridge were also close at 10 mm and 12 mm, respectively. Figures 5.5(b) and 5.6 likewise show good agreement. Comparisons between measured and predicted geogrid strains for different reinforcement layers, shown in Figure 5.7, also indicate reasonable agreement with regard to trend and magnitude. Deviations may reflect the well-known difficulty of trying to measure geogrid strains using foil strain gages.

Lateral earth pressures and vertical stresses within the GRS abutment are shown in Figures 5.8 – 5.14. Figure 5.8 compares the measured and predicted lateral earth pressures behind wall facing at elevation of 4.5 m from top of bedrock during different construction stages, and indicates good agreement with respect to both magnitude and trend. Figures 5.10, 5.11, and 5.12 shows measured and predicted vertical stresses during construction at the base of bridge abutment and at elevations of 2.3 m and 4.1 m. The trend is generally in good agreement, although there were some deviations in magnitude for measured and predicted values. As shown in Figure 5.14, predicted vertical stresses underneath the bridge footing were very close to the estimated values by Abu-Hejleh et al. (2001), but much larger than the measured values. This discrepancy may be due to soil arching effects underneath the bridge footing (Helwany et al. 2003).

The above comparisons indicate that simulated results using FLAC are in reasonable agreement with field measurements, which shows the capability of FLAC to predict the static behavior of GRS bridge abutments. Some of our future work with FLAC will be to perform parametric studies to investigate the effects of different design parameters (e.g., soil modulus, soil friction angle, soil cohesion, reinforcement stiffness, reinforcement length, reinforcement spacing, and bridge load) on the static response of GRS bridge abutments.

Chapter 6 – Numerical Simulations of GRS Retaining Wall for Seismic Loading

6.1 UCSD Shaking Table Test

A field-scale seismic test of a GRS retaining wall was conducted on the LHPOST at UCSD in April 2013. The entire specimen measured $4.62 \times 9.10 \times 6.55$ m, and consisted of facing elements, geogrid reinforcement, foundation soil, and backfill soil. A schematic diagram of the wall specimen is shown in Figure 6.1. A foundation soil layer with thickness = 310 mm was first placed in the large soil confinement box. The soil consisted of clean, angular, well graded sand with no gravel and low fines content (2.8%). The GRS wall was then constructed using 30 courses of facing blocks placed on the leveling pad with a slight setback of 1.6 mm at each level. The blocks were high strength, stackable, masonry units with integrated polymer mechanical connectors to provide positive block-block and block-grid connections. The reinforcement was Tensar UX1400 high-density polyethylene (HDPE) geogrid and was attached to the facing using the integrated connectors. Geogrid layers had a uniform length of 4.27 m and a vertical spacing of 0.61 m starting at the top of the first course of block. The backfill soil was the same as for the foundation and was compacted using a vibratory smooth drum roller. The average dry unit weight for the backfill was 17.3 kN/m^3 , which corresponds to an average relative density of 88% for this material.

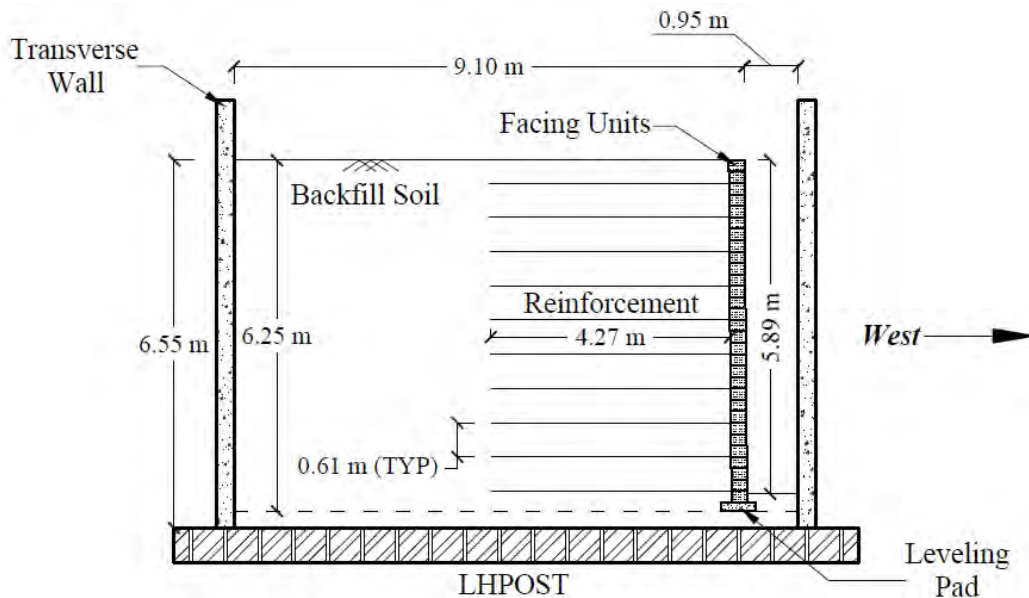


Figure 6.1. GRS wall specimen configuration.

The GRS wall specimen was subjected to a series of harmonic and recorded ground motions interspersed with low amplitude white noise excitation over the course of a three-day period. Harmonic motions were first applied, ranging in frequency from 0.5 Hz to 7 Hz and in amplitude from 0.1g to 0.4g. Recorded ground motions from the 1994 Northridge, 1995 Kobe, and 2010 Maule earthquakes were then applied at various scales up to the force limit of the LHPOST actuators. After the recorded ground motions, another series of harmonic motions was applied to characterize changes in the GRS wall specimen.

6.2 Numerical Simulations

Numerical simulations were performed using FLAC-2D to compare with measurements for the wall. The concrete facing blocks were modeled as elastic materials with modulus $E = 20$ GPa and Poisson's ratio $\nu = 0.2$. The backfill soil was modeled as a linearly-elastic perfectly-plastic dilatant material with a Mohr-Coulomb failure criterion and a non-associated flow rule. Geogrid reinforcement was characterized using cable elements with a tensile stiffness of 600 kN/m (Tensar UX1400). Soil-geogrid interfaces were characterized using $c' = 0$ and $\phi' = 42^\circ$, such that interface sliding was possible. The soil-block and block-block interfaces were modeled using interface elements with zero cohesion and friction angles equal to 28° and 35° , respectively. Soil parameters for the FLAC simulations are summarized in Table 6.1.

Table 6.1. Model parameters for backfill soil.

| γ (kN/m ³) | E (MPa) | ν | c' (MPa) | ϕ' (°) | ψ (°) |
|----------------------------------|--------------|-------|---------------|-------------|------------|
| 17.6 | 13 | 0.3 | 20 | 42 | 8 |

The numerical simulations consisted of a static analysis stage (including construction sequence), followed by a dynamic loading stage. For the static analysis, foundation soil was placed first and the GRS wall was then “constructed” as 30 individual lifts. The soil-block and block-block interfaces were placed at specified positions and the geogrid layers were rigidly connected to the facing blocks at appropriate elevations. Gravity loads were applied to the system between each lift. Dynamic analysis was performed for conditions starting at the end of static loading but, due to the complexity of the complete loading history, only included a portion of the dynamic shaking that occurred for this retaining wall. Earthquake excitations, including 50% Kobe, 25% Northridge, and 50% Northridge earthquake records, were applied to the bottom boundary in sequence. FLAC was used to predict lateral facing displacement profiles for the 50% Northridge earthquake. Figure 6.2 shows a comparison of the FLAC results with measurements taken on the GRS wall for the same event.

6.3 Simulation Results

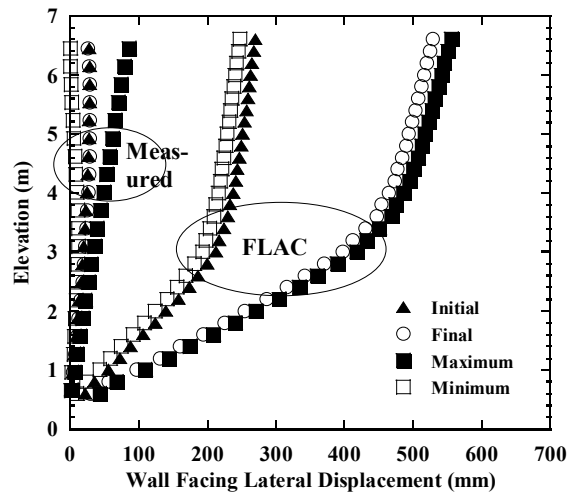


Figure 6.2. Predicted and measured wall lateral facing displacements for 50% Northridge record (FLAC model was pre-shaken with 50% Kobe and 25% Northridge records).

6.4 Summary

Measured and predicted values for initial lateral displacements before shaking, minimum and maximum lateral displacements during shaking, and final lateral displacements after shaking are shown in Figure 6.2. FLAC significantly overestimated the lateral displacements of the wall facing during seismic loading. The actual shaking history of GRS wall was complicated and consisted of a large number of white noise motions, harmonic motions and scaled earthquake ground motions before the application of the 50% Northridge record. To reduce the long computation time in FLAC, only a few of these motions were applied prior to the 50% Northridge record. This is the likely explanation for discrepancies in Figure 6.2. Regardless, this exercise has indicated that FLAC may be more likely to overpredict, rather than underpredict, displacement measurements for GRS structures under seismic loading conditions.

Chapter 7 – Numerical Simulations of Seismic Response of GRS Abutments in Longitudinal Direction

7.1 Numerical Model

7.1.1 Model Geometry

FLAC-2D was used to simulate the response of a 150 ft. bridge with GRS abutments to longitudinal shaking for the 1994 Northridge earthquake. The model is two-dimensional, thus a 1 ft. thick slice (perpendicular to page) is considered with the same bridge seat vertical contact pressure as the prototype. The abutments were modeled using properties for a high-capacity, commercially available geogrid and properties for typical abutment soils in California. The geometry of the FLAC model is shown in Figure 7.1. The foundation soil is 10 ft. deep below the abutments. Each abutment has a total height 20.8 ft., consisting of a 12.8 ft.-high lower GRS wall and an 8 ft.-high upper abutment wall. The lower wall has modular block concrete facing elements that measure 0.64 ft. (width) \times 0.64 ft. (height). The length of geogrid reinforcement is 20.8 ft. ($1H$) for both the lower and upper walls. The bearing bed (secondary) reinforcement in the lower wall has a length of 10.4 ft. ($0.5H$). The vertical spacing of geogrid layers is 0.64 ft. for the lower wall and 1 ft. for the upper wall. The prototype bridge deck is 150 ft. long, 40 ft. wide, and 6.5 ft. high, and has a total weight of 1680 kips (840 kips per abutment). The bridge seat has a loaded width of 8 ft. and is offset 1 ft. from the back of lower wall facing. There is a 1-inch expansion joint (gap) between the bridge and bridge seat backwall. The bridge clearance height is 14.3 ft., which satisfied the FHWA minimum requirement of 14 ft. (Stein and Neuman 2007). Lateral boundaries for the model are located at a distance of 83.2 ft. ($4H$) behind the lower wall facing to minimize the influence of boundary conditions on the results. The FLAC mesh and configuration details for the model are shown in Figures 7.2 and 7.3, respectively.

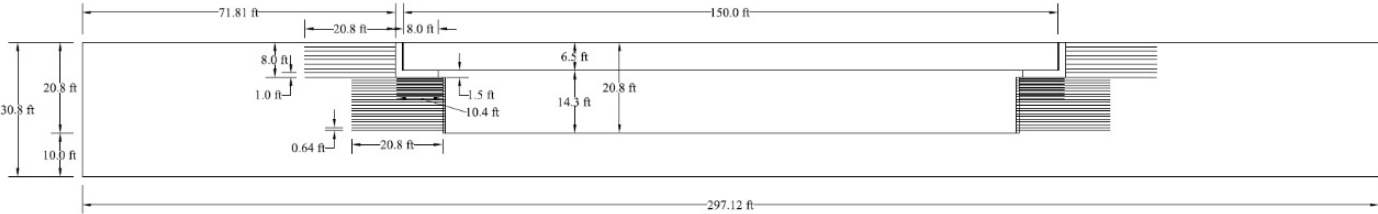


Figure 7.1. Geometry for GRS-supported bridge model with shaking in longitudinal direction.



Figure 7.2. FLAC mesh for GRS-supported bridge model with shaking in longitudinal direction.

7.2 Static Analysis

A typical construction sequence was included in the static analysis. Foundation soil was placed first, and then both GRS abutments were “constructed” at the same time. The concrete blocks and soil were placed on the foundation soil in 20 lifts to form the lower GRS walls – one layer at a time with gravity applied after each lift. The soil-block and block-block interfaces were placed at specified positions and the geogrid layers were rigidly connected to the facing blocks at appropriate elevations. For field structures, the top three courses of facing blocks are usually grouted together to maximize local stability. A large tensile strength was assigned to the interfaces between these three blocks to numerically simulate these grouting effects. The concrete bridge seats were placed on top of the GRS backfill soils, and the bridge superstructure was then placed directly on bridge seats. The average vertical pressure applied on each abutment is 2,625 psf. Finally, the bridge approaches were constructed using wrapped-face geotextile reinforced-soil layers to create a smooth transition between the bridge and approach roadways. Geogrid and wrapped-face geotextile layers were placed at appropriate elevations during construction. Bearing bed (secondary) reinforcements (8 layers) were included near the top of each GRS wall. Static analysis indicated that both abutments have the same behavior due to symmetry of the applied loading. Lateral boundaries of the numerical model were fixed in the horizontal direction and free to move in the vertical direction, whereas the bottom boundary was fixed in both horizontal and vertical directions.

7.3 Seismic Analysis

Seismic loading was performed for conditions starting at the end of static loading. The 1994 Northridge earthquake ground motion measured at the Newhall Station (PGA = 0.58 g), shown in Figure 7.4, was applied at the bottom boundary in the longitudinal direction. Simulation results are not symmetrical for the two abutments due to the asymmetry of dynamic loading. Free-field conditions were imposed at the lateral boundaries to absorb seismic waves and prevent them from reflecting back into the problem domain.

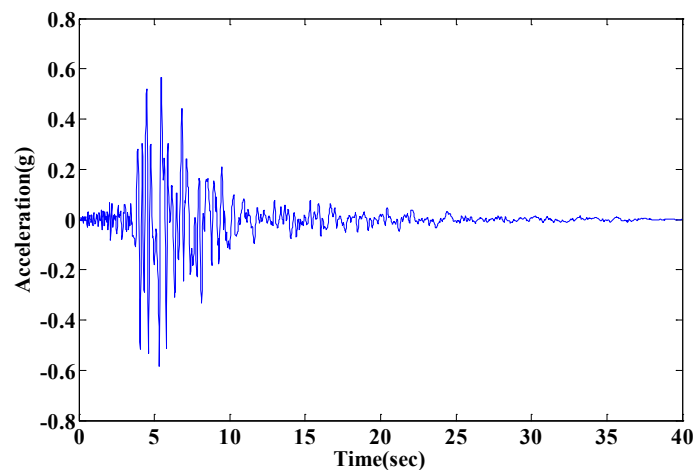


Figure 7.4. Acceleration time history for 1994 Northridge Earthquake – Newhall Station.

7.4 Simulation Results for Base Case

Key numerical results for the GRS bridge abutments for the base case, as previously described, are presented in Table 7.2. Each value represents an average displacement for the two abutments. Table 7.2 indicates that, for longitudinal ground motion, the maximum seismic-induced displacement for the wall facing is about 2 in., settlement of the bridge seat is less than 1 in., and a lateral movement of the bridge seat is about 2.5 in.

Table 7.2. Key displacements of GRS bridge abutments (in.) for base case conditions.

| | Maximum Lateral Displacement of Wall Facing | Settlement of Bridge Seat | Lateral Displacement of Bridge Seat |
|-----------------------------------|---|---------------------------|-------------------------------------|
| Static | 0.389 | 1.601 | 0.079 |
| Seismic (total, including static) | 2.24 | 2.257 | 2.527 |
| Seismic-Induced | 2.025 | 0.656 | 2.448 |

Note: maximum static and maximum seismic-induced lateral displacements do not sum to maximum total lateral displacements because these values occur at different elevations on the wall.

7.5 Parametric Studies

Parametric studies were then conducted, as deviations from the base case, to investigate the effects of reinforcement spacing, reinforcement stiffness, reinforcement length, soil cohesion, soil friction angle, bridge load, earthquake ground motion record, and bearing pad friction coefficient on settlement of the bridge seat and maximum lateral displacement of the lower wall facing. Results are presented in the following figures and discussed at the end of this chapter.

7.5.1 Reinforcement Spacing

Table 7.3. Maximum lateral displacement of GRS wall facing (in).

| Reinforcement Spacing (in.) | 8 | 16 |
|-----------------------------------|-------|-------|
| Static | 0.389 | 0.468 |
| Seismic (total, including static) | 2.24 | 3.504 |
| Seismic-Induced | 2.025 | 3.036 |

Note: maximum static and maximum seismic-induced lateral displacements do not sum to maximum total lateral displacements because these values occur at different elevations on the wall.

Table 7.4. Settlement of bridge seat (in).

| Reinforcement Spacing (in.) | 8 | 16 |
|-----------------------------------|-------|-------|
| Static | 1.601 | 1.625 |
| Seismic (total, including static) | 2.257 | 2.441 |
| Seismic-Induced | 0.656 | 0.816 |

Table 7.5. Lateral movement of bridge seat (in).

| Reinforcement Spacing (in.) | 8 | 16 |
|-----------------------------------|-------|-------|
| Static | 0.079 | 0.112 |
| Seismic (total, including static) | 2.527 | 2.574 |
| Seismic-Induced | 2.448 | 2.462 |

7.5.2 Reinforcement Stiffness

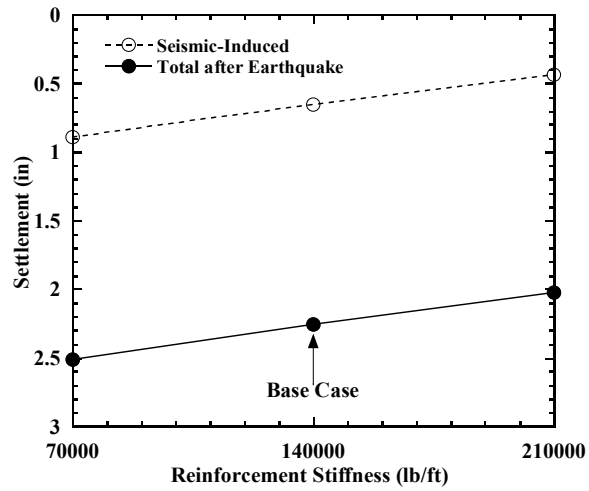


Figure 7.5. Effect of reinforcement stiffness on average settlement of bridge seat.

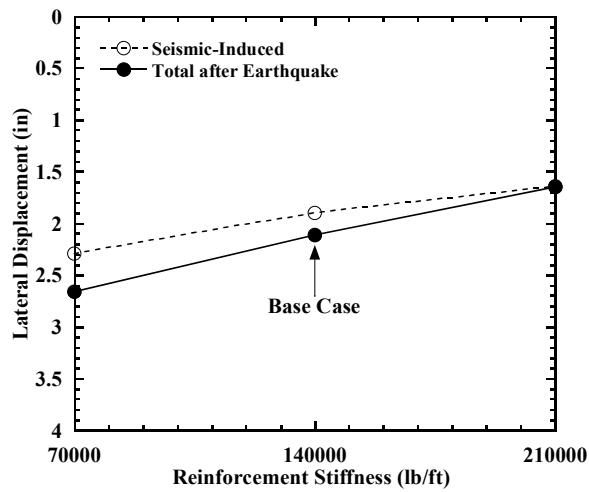


Figure 7.6. Effect of reinforcement stiffness on maximum lateral displacement of lower wall facing.

7.5.3 Reinforcement Length

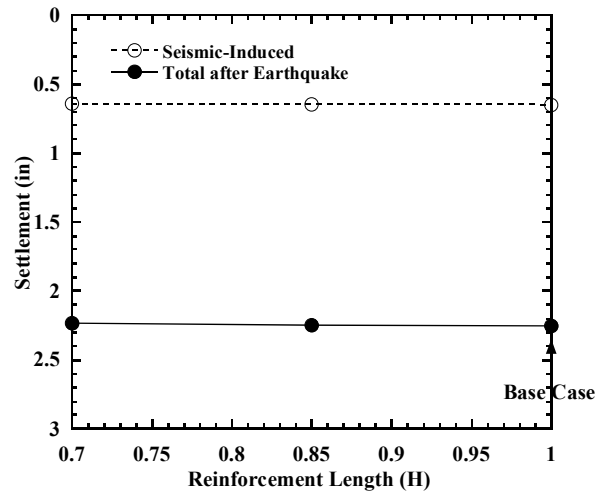


Figure 7.7. Effect of reinforcement length on average settlement of bridge seat.

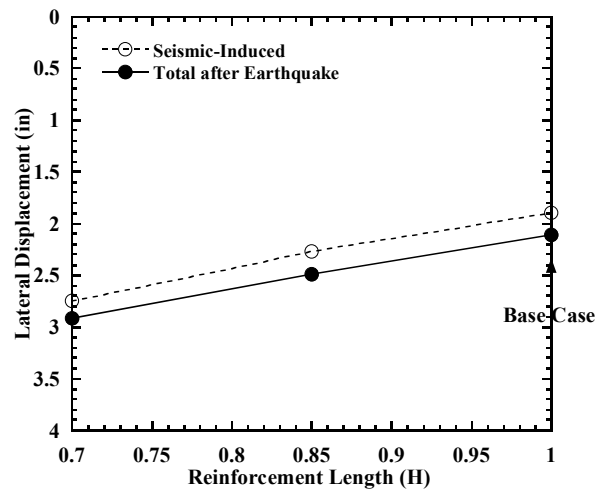


Figure 7.8. Effect of reinforcement length on maximum lateral displacement of lower wall facing.

7.5.4 Soil Cohesion

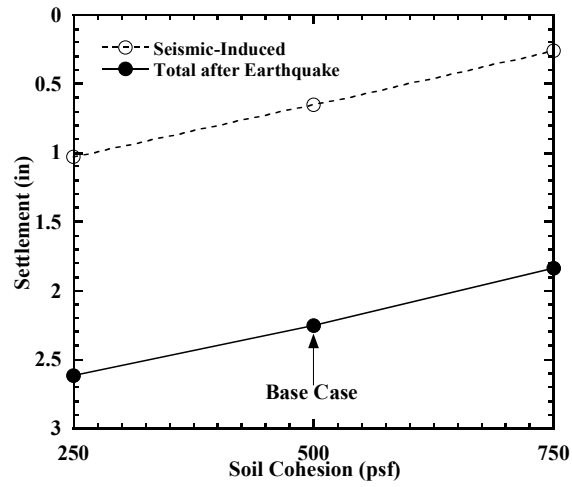


Figure 7.9. Effect of soil cohesion on average settlement of bridge seat.

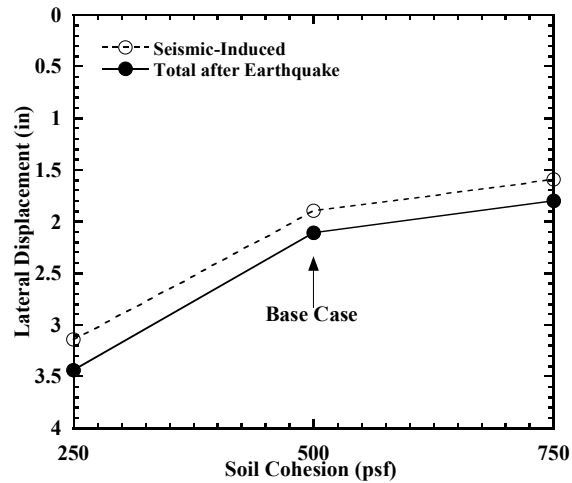


Figure 7.10. Effect of soil cohesion on maximum lateral displacement of lower wall facing.

7.5.5 Soil Friction Angle

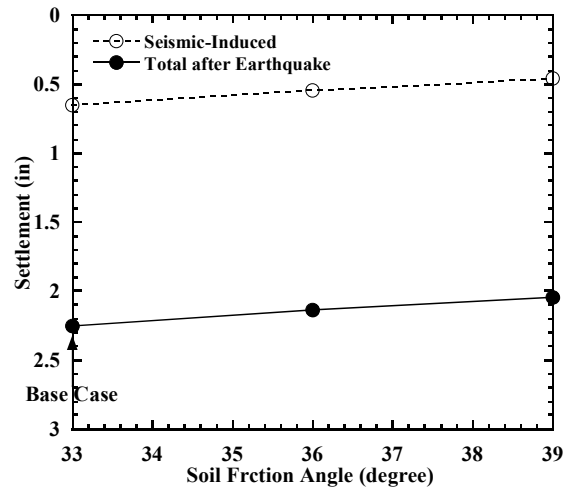


Figure 7.11. Effect of soil friction angle on average settlement of bridge seat.

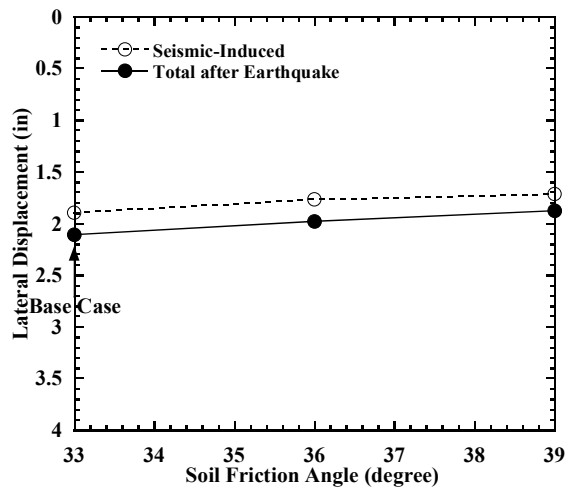


Figure 7.12. Effect of soil friction angle on maximum lateral displacement of lower wall facing.

7.5.6 Bridge Load

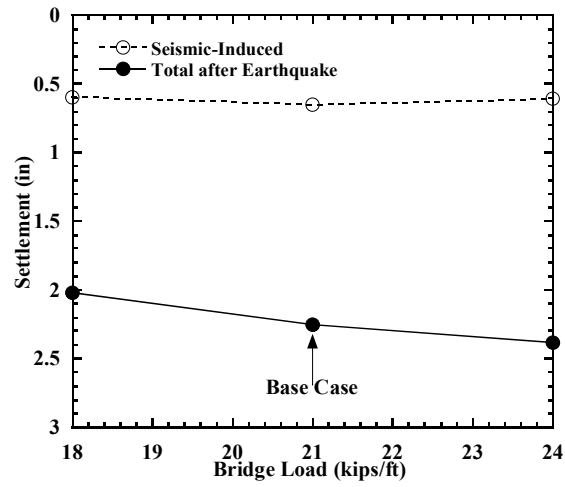


Figure 7.13. Effect of bridge load on average settlement of bridge seat.

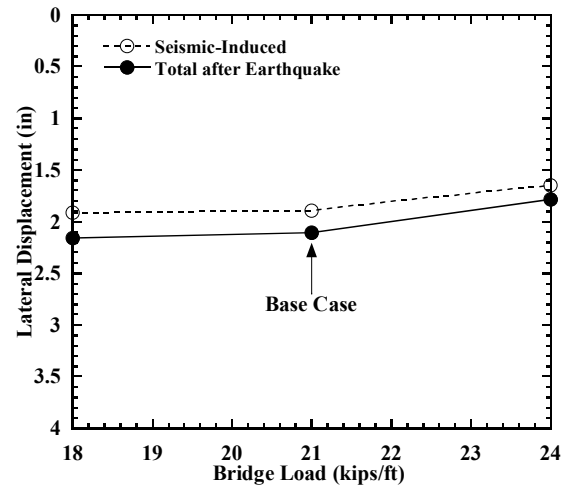


Figure 7.14. Effect of bridge load on maximum lateral displacement of lower wall facing.

7.5.7 Earthquake Ground Motion Record

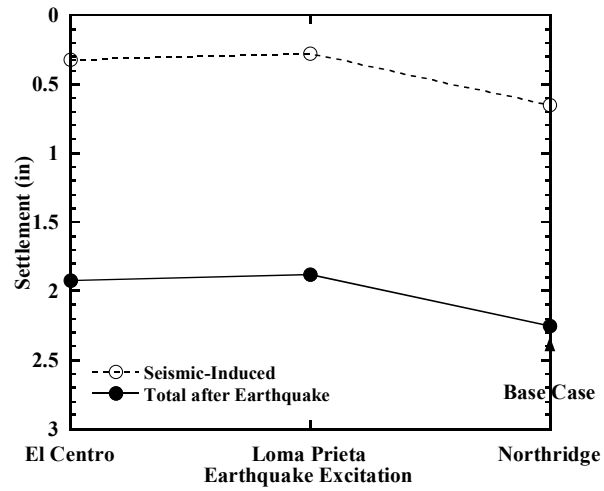


Figure 7.15. Effect of earthquake ground motion record on average settlement of bridge seat.

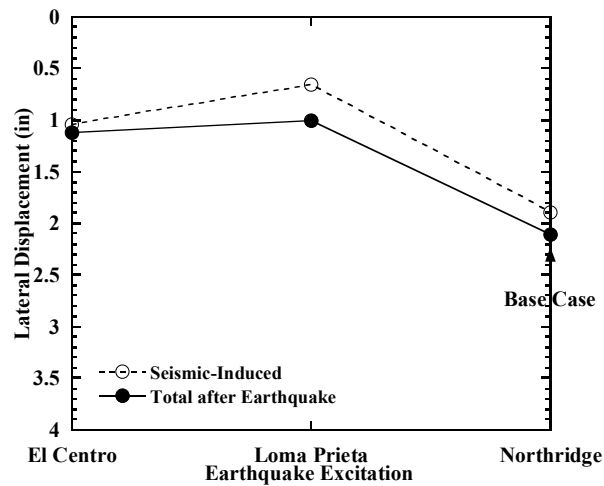


Figure 7.16. Effect of earthquake ground motion record on maximum lateral displacement of lower wall facing.

7.5.8 Bridge Bearing Pad Friction Coefficient

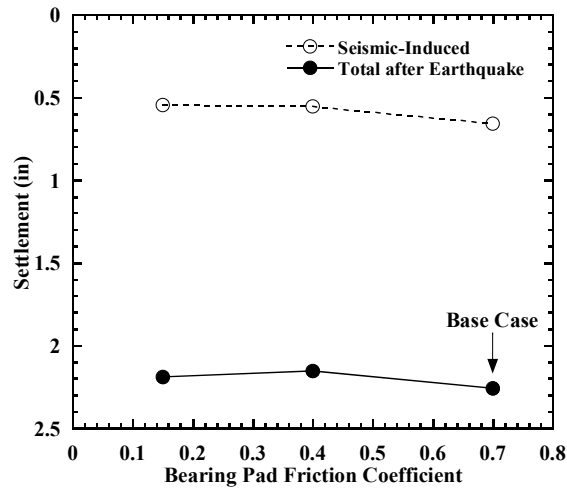


Figure 7.17. Effect of bearing pad friction coefficient on average settlement of bridge seat.

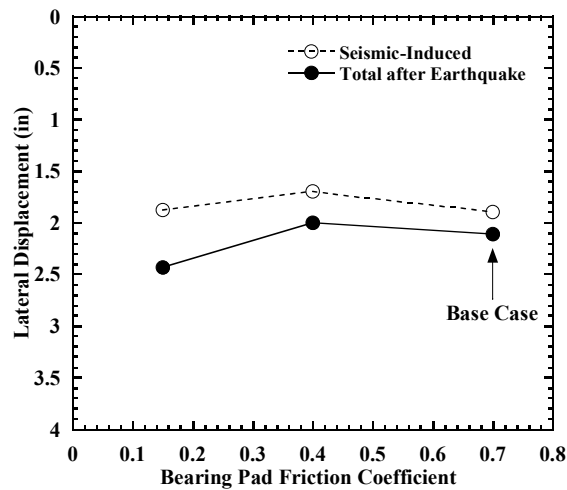


Figure 7.18. Effect of bearing pad friction coefficient on maximum lateral displacement of lower wall facing.

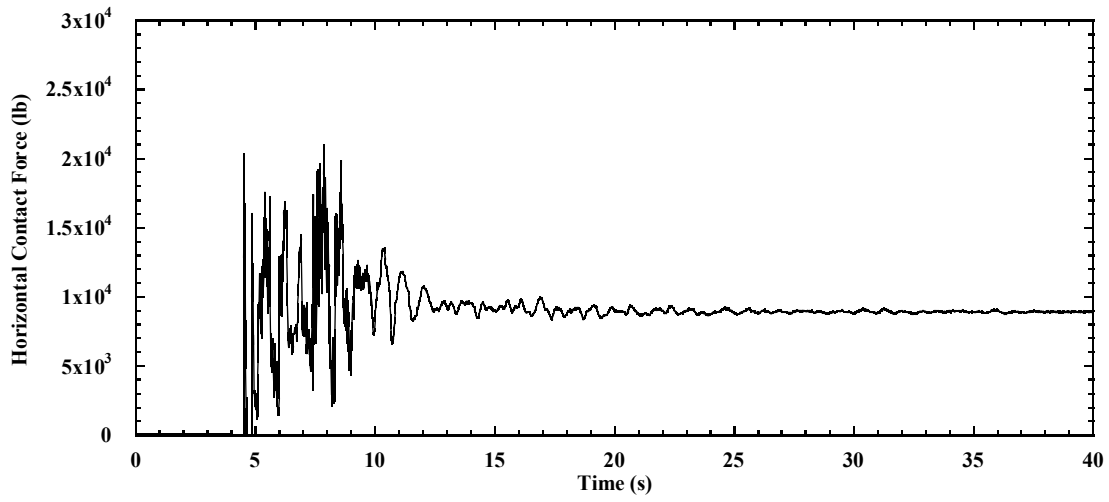


Figure 7.19. Horizontal contact force on left bridge seat backwall for bearing friction coefficient = 0.15.

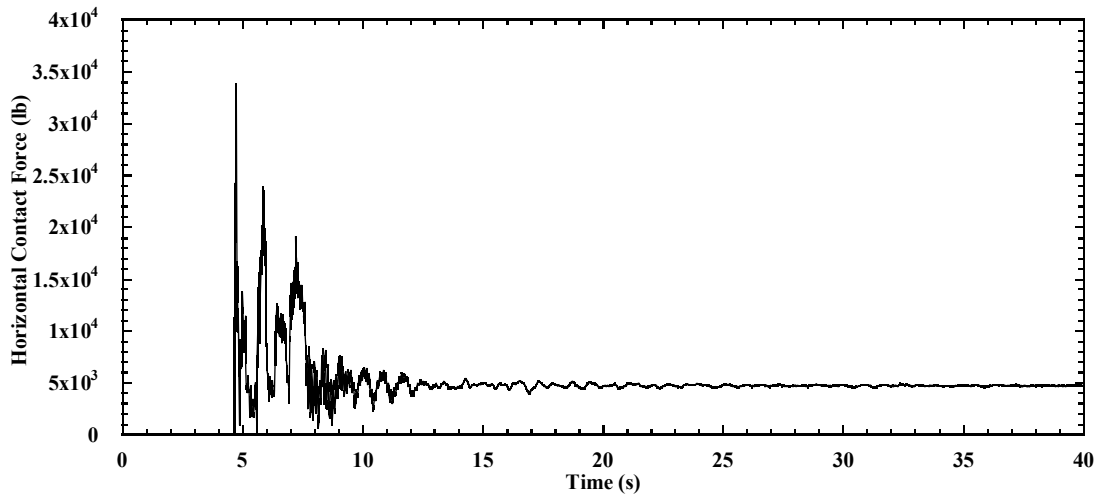


Figure 7.20. Horizontal contact force on right bridge seat backwall for bearing friction coefficient = 0.15.

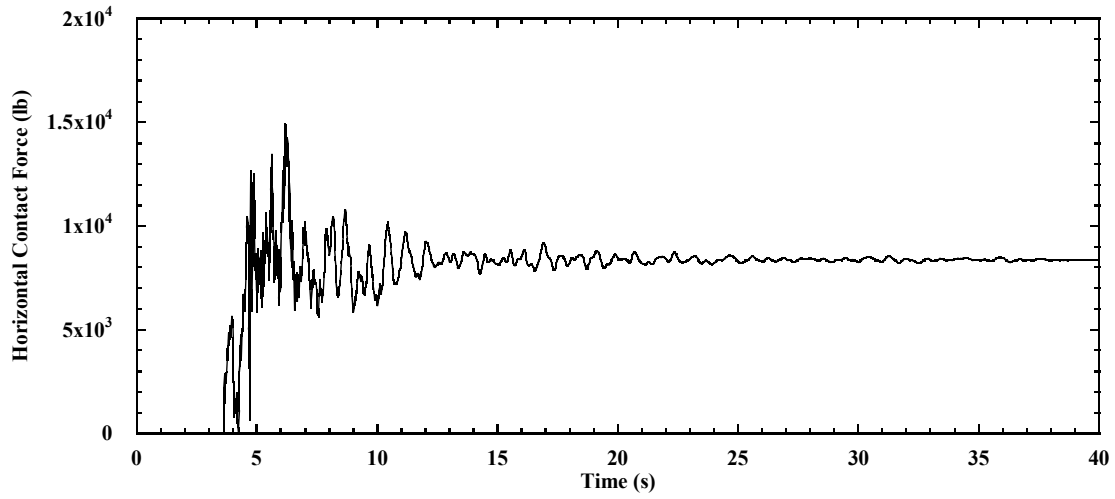


Figure 7.21. Horizontal contact force on left bridge seat backwall for bearing friction coefficient = 0.4.

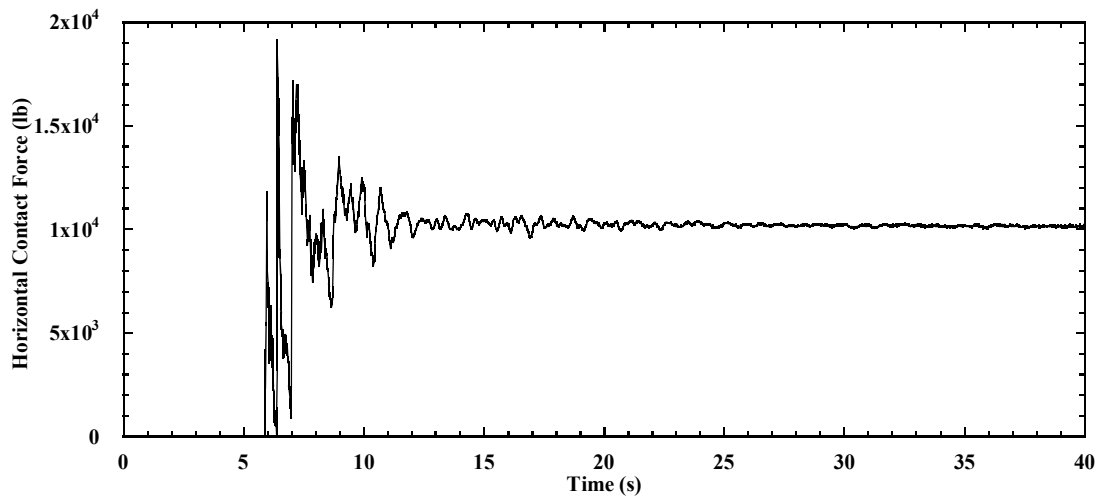


Figure 7.22. Horizontal contact force on right bridge seat backwall for bearing friction coefficient = 0.4.

7.6 Summary

Key numerical results in Table 7.2 indicate that lateral displacements of the wall facing and settlements and lateral displacements of the bridge seat are small for the base case with shaking in the longitudinal direction, and would likely be considered acceptable for a major earthquake such as Northridge. In particular, values of seismic-induced settlement are 0.65 in., which would generally not be expected to cause serious distress to a single-span or multi-span bridge.

Results of the parametric studies indicate that reinforcement stiffness and soil cohesion have significant influences on the seismic-induced settlement of the bridge seat. Interestingly, reinforcement length had an effect on lateral displacement of the wall facing but not on settlement of the bridge seat. A possible explanation is that a minimum reinforcement length of $0.7H$ is sufficiently long to reduce settlement, as this length is beyond the location where the bridge seat is placed for the GRS abutments considered, and any length beyond this is unimportant for settlement analysis. Reinforcement spacing had significant effects on lateral displacement of the wall facing (Tables 7.3-7.5). In the FHWA design guideline (Wu et al. 2006), the maximum allowable reinforcement spacing for GRS abutments with flexible facing is 16 in. For GRS-IBS, which is a special type of GRS abutment with flexible facing, the spacing is limited to 8 in. The results indicate that close reinforcement spacing in the vertical direction is preferred for seismic design.

As can be seen in Figure 7.9, seismic-induced settlement of the bridge seat for the case with soil cohesion = 750 psf was three times smaller than the case with soil cohesion = 250 psf. Soil cohesion also played an important role in seismic-induced lateral displacement of the wall facing, as shown in Figure 7.10. Ling et al. (2012) also found that soil cohesion can improve seismic performance of GRS walls constructed using fine-grained soils. However, they suggested that apparent (i.e., unsaturated) cohesion might vary significantly due to environmental changes during the service life of GRS walls. Soil friction angle had a small effect on seismic-induced displacements.

As shown in Figure 7.13, increasing the bridge load produced higher settlements for static conditions, as expected, but had little effect on seismic-induced settlement. Also, increasing the bridge load actually reduced lateral displacements of the wall, which is due to the additional confinement (and thus strength) of the GRS abutment structures.

Figures 7.15 and 7.16 show that the 1994 Northridge earthquake, Newhall station, record produced the highest displacements. For less destructive earthquake records, such as 1940 Imperial Valley earthquake, El Centro station (PGA = 0.31 g) and 1989 Loma Prieta earthquake, Capitola station (PGA = 0.53 g), seismic-induced settlements of the bridge seat were approximately 0.3 in. and seismic-induced maximum lateral displacements of the wall facing were less than 1 in. For Northridge, these values increased to 0.65 in. and 2 in., respectively.

For the simulations with variable bearing pad friction coefficient, sliding occurred with friction coefficient = 0.15 under static loading, which produced a slightly larger facing lateral displacement. No sliding occurred under static loading for higher friction coefficients. After seismic loading, Figure 7.17 shows that the seismic-induced bridge seat settlement is only slightly larger for a high friction coefficient of 0.7. Figure 7.18 shows that lateral displacement was similarly insensitive to friction coefficient. The 1-inch expansion joint closed at approximately 5 seconds during shaking for bearing pad friction coefficients = 0.15 and 0.4, whereas no closure (and thus no contact force) occurred for friction coefficient = 0.7. The maximum horizontal contact force between the bridge and the bridge seat backwall occurred for the right-side abutment and was equal to approximately 34,000 lb. for friction coefficient = 0.15 and 19,000 lb. for friction coefficient = 0.4. Since the height of the backwall in contact with the bridge deck is 6.5 ft., the maximum average compressive stress on the backwall is 36.3 psi (34,000 lb./6.5 ft./144), which is well below the minimum expected compressive strength of 3,000 psi for the concrete. Even if the bridge seat is prevented from sliding at the base, the maximum shear stress on the backwall (thickness = 1.5 ft.) will be 157.4 psi (34,000 lb./1.5 ft./144), which is at most one-half of the expected shear strength for 3,000-psi concrete.

Considering all conditions for the parametric studies, settlements of the bridge seat were approximately 2 in. at the end of construction, and seismic-induced settlements of bridge seat varied between 0.3 in. to 1 in., depending on reinforcement geometry, soil and reinforcement properties, bridge load, and earthquake ground motion record. Lateral displacements of wall facing were also small at the end of construction, and seismic-induced lateral displacements of wall facing were typical less than 3 in.

Chapter 8 – Comparison of FLAC and ABAQUS Results for Seismic Response of GRS Bridge Abutments in Longitudinal Direction

8.1 Numerical Model

8.1.1 Model Geometry

FLAC and ABAQUS were used to model a 150 ft. bridge with GRS abutments as a check on FLAC. The model geometry for this comparison study is shown in Figure 8.1. The foundation soil is 10 ft. deep below the abutment structure. The total abutment height is 20.8 ft., which consisted of a 12.8 ft.-high lower GRS wall and an 8 ft.-high upper abutment wall. The lower wall has modular block concrete facing elements that measure 0.64 ft. (width) \times 0.64 ft. (height). Geogrid reinforcement for the lower wall has a length of 20.8 ft. ($1H$) and a vertical spacing of 0.64 ft. The bridge seat has a loaded width of 8 ft. and an offset of 1 ft. from the back of lower wall facing. The bridge deck is 150 ft. long, 40 ft. wide and 6.5 ft. high, and has a total weight of 1680 kips. Abutment details are shown in Figure 8.2. The model for this comparison study has three differences from the longitudinal base case described in Figures 7.1 and 7.3; there is no soil reinforcement behind the upper wall or secondary soil reinforcement behind the lower wall and the model was “constructed” all at once for static analysis.

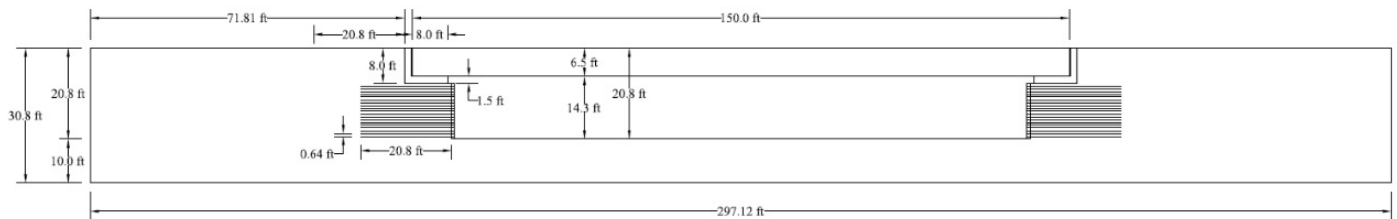


Figure 8.1. Geometry of GRS-supported bridge for comparison of FLAC and ABAQUS results.

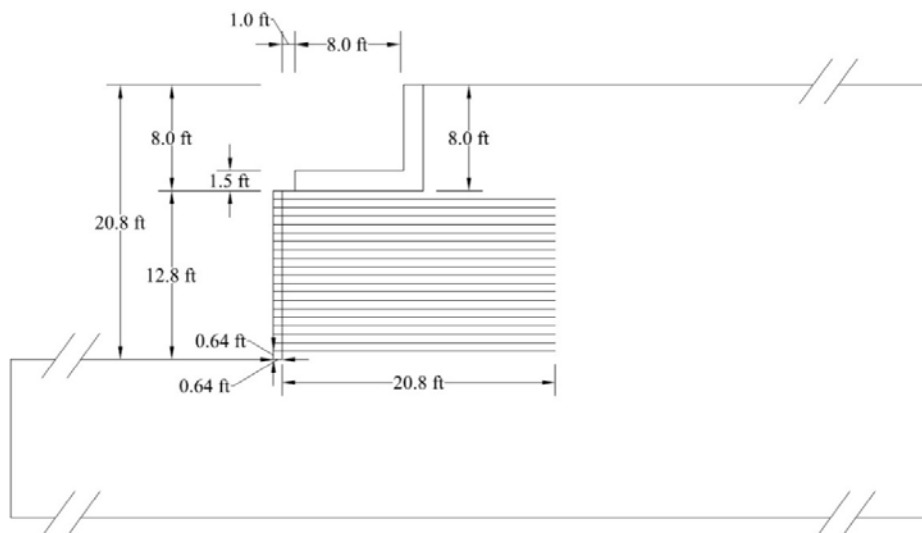


Figure 8.2. Configuration details of GRS bridge abutment #2.

8.1.2 Numerical Meshes and Boundary Conditions

The numerical model meshes for FLAC and ABAQUS are shown in Figure 8.3 and Figure 8.4. Lateral boundaries were located at a distance of 83.2 ft. ($4H$) behind the lower wall facings to minimize the influence of boundary conditions on the results. Lateral boundaries were fixed in the horizontal direction and free to move in the vertical direction, whereas the bottom boundary was fixed in both horizontal and vertical directions for both programs.



Figure 8.3. FLAC mesh for GRS bridge abutment comparison study.



Figure 8.4. ABAQUS mesh for GRS bridge abutment comparison study.

8.1.3 Material Models and Properties

The concrete facing blocks, bridge seat, and bridge decks were modeled as elastic materials with modulus $E = 500,000$ ksf and Poisson's ratio $\nu = 0.2$. The backfill soil was modeled as a linearly-elastic perfectly-plastic dilatant material with a Mohr-Coulomb failure criterion and a non-associated flow rule. The backfill soil properties were the same as presented in Table 7.1 (Earth Mechanics 2005). The foundation soil was assumed to have the same properties as the backfill soil. Geogrid reinforcement with a tensile stiffness = 140,000 lb./ft. was simulated using cable elements in FLAC and truss elements in ABAQUS. The soil-block, block-block, and soil-bridge seat interfaces were modeled using interface elements with no cohesion and frictional angles equal to 22° , 35° , and 22° , respectively.

8.2 Modeling Procedures

As the purpose of this study was to compare the seismic response of GRS bridge abutments using FLAC and ABAQUS, the static construction sequence was not considered to reduce computation time. Therefore, the GRS wall, bridge seat, upper wall, and bridge deck were placed at one time prior to seismic loading. The geogrid reinforcement was rigidly connected to the facing blocks and attached to the soil elements, thus sliding between soil and reinforcement was neglected for these simulations. Bathurst and Hatami (1998) found that this assumption was reasonable, as soil-reinforcement sliding was very small and could be ignored in their study. The bridge deck applied a vertical pressure of 2,625 psf on each abutment. The Northridge

earthquake record (PGA = 0.58 g) was applied to the bottom boundary of each model in the longitudinal direction. The acceleration time history was the same as shown in Figure 7.4.

8.3 Results

Numerical results for maximum lateral displacements of GRS wall facings, settlements of the bridge seats, and lateral displacements of the bridge seats, as obtained using FLAC and ABAQUS for different stages of analysis, are presented below. Displacements in the tables again represent average values for the two abutments.

Table 8.1. Comparison of Maximum Lateral Displacements for GRS Wall Facing (in.).

| | FLAC | ABAQUS |
|-----------------|-------|--------|
| Static | 0.21 | 0.36 |
| Dynamic | 1.957 | 2.502 |
| Seismic-Induced | 1.905 | 2.321 |

Note: maximum static and maximum seismic-induced lateral displacements do not sum to maximum dynamic (total) lateral displacements because these values occur at different elevations on the wall.

Table 8.2. Comparison of Settlements for Bridge Seat (in.).

| | FLAC | ABAQUS |
|-----------------|-------|--------|
| Static | 2.322 | 2.548 |
| Dynamic | 2.893 | 3.168 |
| Seismic-Induced | 0.571 | 0.62 |

Table 8.3. Comparison of Lateral Displacements for Bridge Seat (in.).

| | FLAC | ABAQUS |
|-----------------|-------|--------|
| Static | 0.127 | 0.108 |
| Dynamic | 2.921 | 2.421 |
| Seismic-Induced | 2.794 | 2.313 |

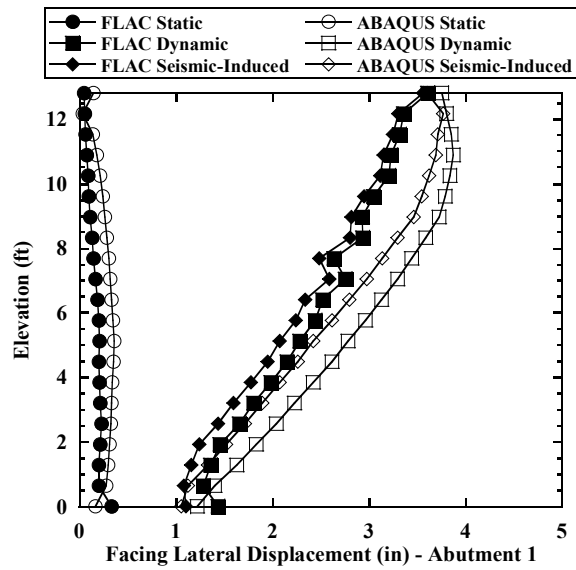


Figure 8.5. Comparison of lateral facing displacement profiles for abutment #1 (left side).

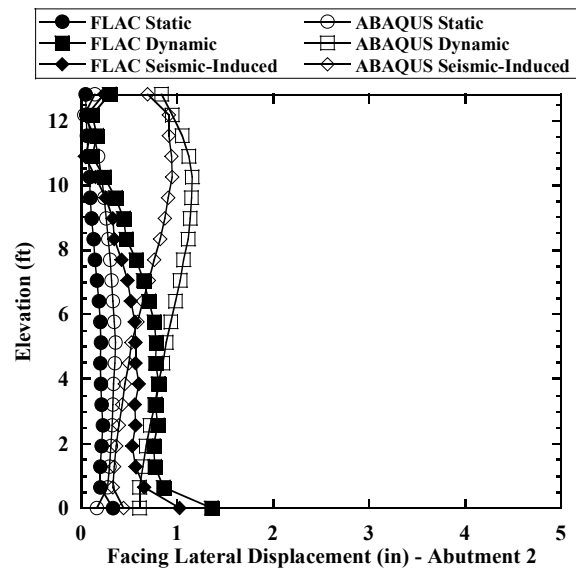


Figure 8.6. Comparison of lateral facing displacement profiles for abutment #2 (right side).

8.4 Summary

The results presented in Tables 8.1, 8.2, and 8.3 are in good agreement and indicate that FLAC and ABAQUS produce similar values of displacement for the same GRS-supported bridge subjected to the same longitudinal ground motion. This agreement lends credibility to the FLAC results presented throughout this report.

Lateral wall displacement profiles, shown in Figures 8.5 and 8.6, are likewise in reasonable agreement for the two programs. FLAC and ABAQUS displacement profiles for abutment #1 are a good match with respect to both magnitude and trend and indicate that ABAQUS gives slightly higher values near the top of the wall. Displacement profiles for abutment #2 are in lesser agreement; however, the total magnitude of displacement is less than 1 in. for both simulations.

Chapter 9 – Numerical Simulations of Seismic Response of GRS Abutments in Transverse Direction

9.1 Numerical Model

9.1.1 Model Geometry

Numerical simulations were also conducted using FLAC-2D for the same model as the longitudinal base case in Fig. 7.1, but with the Northridge ground motion applied in the transverse (cross) direction. Two transverse GRS abutment configurations were simulated; one abutment with two shear keys under the bridge seat and no upper GRS wall, and one abutment with an upper GRS wall and no shear keys, as shown in Figures 9.1 and 9.2, respectively. The foundation soil is 10 ft. deep below the abutment structures. The total height of each abutment is 20.8 ft. and the lower GRS walls are 12.8 ft. high. The lower walls have modular block concrete facing elements (0.64 ft. × 0.64 ft.). Geogrid reinforcement has a length of 20.8 ft. (1H) and a vertical spacing of 0.64 ft. The bridge deck is 150 ft. long, 40 ft. wide, and 6.5 ft. high, and has a total weight of 1680 kips. The width of the bridge seat is 40 ft. in the transverse direction. The side boundaries are located at a distance of 41.6 ft. (2H) from the lower wall facing. The meshes for the FLAC simulations are shown in Figures 9.3 and 9.4. FLAC-2D was used to model a 1 ft. slice (perpendicular to page) with the same bridge seat vertical contact pressure as the prototype.

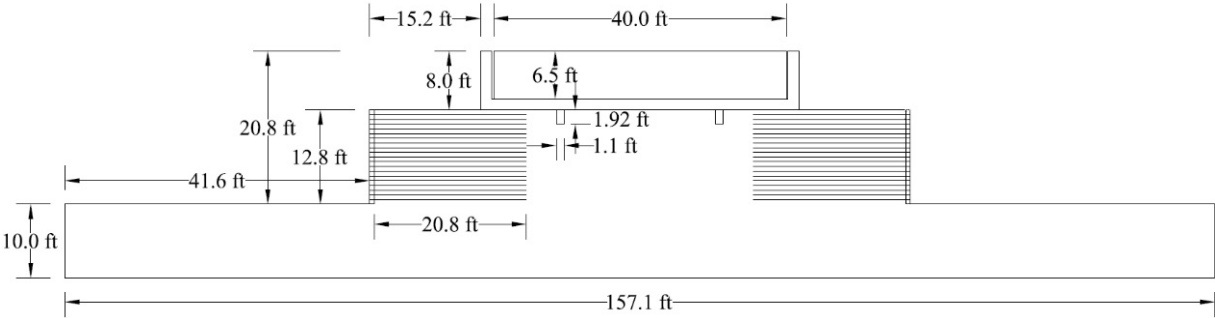


Figure 9.1. Geometry of GRS bridge abutment model with shear key in transverse direction.

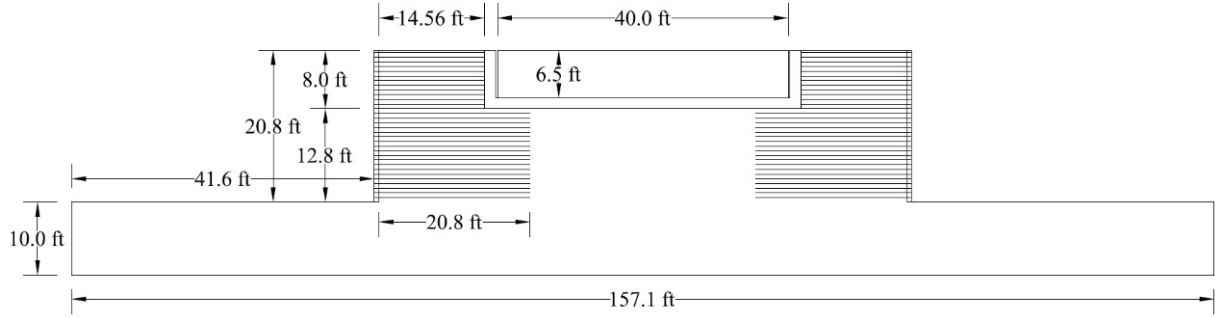


Figure 9.2. Geometry of GRS bridge abutment model without shear key in transverse direction.

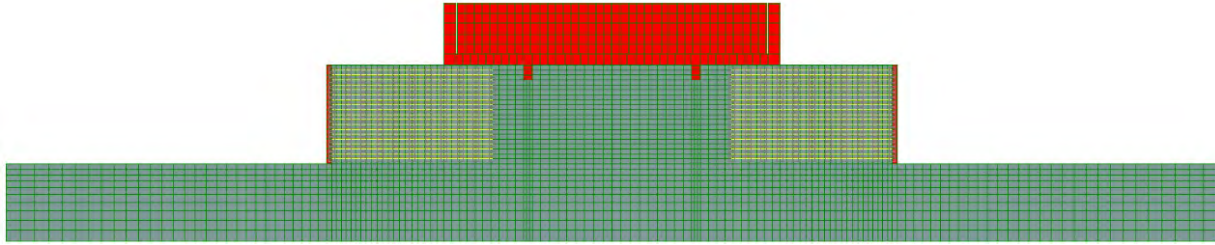


Figure 9.3. FLAC mesh for GRS bridge abutment model with shear key in transverse direction.

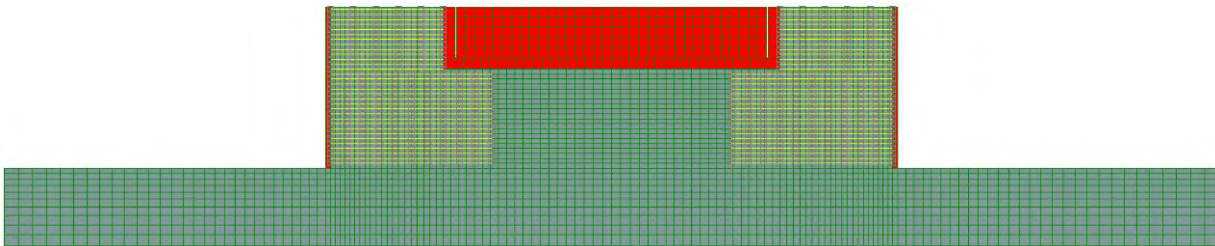


Figure 9.4. FLAC mesh for GRS bridge abutment model without shear key in transverse direction.

9.1.2 Material Models and Properties

The concrete facing blocks, bridge seat, and bridge decks were modeled as elastic materials with modulus $E = 500,000$ ksf and Poisson's ratio $\nu = 0.2$. The backfill soil was modeled as a linearly-elastic perfectly-plastic dilatant material with a Mohr-Coulomb failure criterion and a non-associated flow rule. Soil properties are the same as presented in Table 7.1 and correspond to typical backfill soil conditions for bridge abutments in California (Earth Mechanics 2005). The foundation soil was assumed to have the same characteristics as the backfill soil. Geogrid reinforcement was simulated using cable elements with tensile stiffness = 140,000 lb./ft. The soil-geogrid interfaces were characterized using $c' = 0$ and $\phi' = 33^\circ$, such that interface sliding was possible. The soil-block, block-block, and soil-bridge seat interfaces were modeled using interface elements with no cohesion and frictional angles equal to 22° , 35° , and 22° , respectively.

9.2 Static Analysis

The same construction sequence as for the longitudinal case was included in the static analysis. Foundation soil was first placed. Concrete blocks and soil for the GRS abutments were then placed on the foundation soil in 20 lifts for the lower GRS walls – one layer at a time with gravity applied after each lift. The soil-block and block-block interfaces were placed at specified positions and the geogrid layers were rigidly connected to the facing blocks at appropriate elevations. The concrete bridge seat was placed on top of the GRS backfill soil, and the bridge superstructure was then placed directly on bridge seat. The average vertical pressure applied on

the abutment was again 2,625 psf. The upper GRS walls (Figure 9.2) were also constructed in lifts. Lateral boundaries were fixed in the horizontal direction and free to move in the vertical direction, whereas the bottom boundary was fixed in both horizontal and vertical directions.

9.3 Seismic Analysis

Seismic loading was performed for conditions starting at the end of static loading. The Northridge earthquake ground motion (PGA = 0.58 g), shown in Figure 7.4, was applied to the bottom boundary in the longitudinal direction. Free-field conditions were imposed at the lateral boundaries to absorb seismic waves and prevent them from reflecting back into the problem domain.

9.4 Simulation Results

Numerical results for the two types of GRS bridge abutments with transverse loading, including maximum lateral displacement of GRS wall facing, settlement of bridge seat, and seismic-induced lateral displacement of bridge seat, are presented in Tables 9.1, 9.2, and 9.3, respectively.

Table 9.1. Maximum lateral displacement of GRS wall facing (in.).

| | W/ Shear Key | W/O Shear Key |
|-----------------|--------------|---------------|
| Static | 0.572 | 0.639 |
| Dynamic | 3.446 | 4.107 |
| Seismic-Induced | 2.902 | 3.897 |

Note: maximum static and maximum seismic-induced lateral displacements do not sum to maximum dynamic (total) lateral displacements because these values occur at different elevations on the wall.

Table 9.2. Settlement of bridge seat (in.).

| | W/ Shear Key | W/O Shear Key |
|-----------------|--------------|---------------|
| Static | 2.077 | 1.912 |
| Dynamic | 2.722 | 2.781 |
| Seismic-Induced | 0.645 | 0.869 |

Table 9.3. Seismic-induced lateral movement of bridge seat (in.).

| | W/ Shear Key | W/O Shear Key |
|-----------------|--------------|---------------|
| Seismic-Induced | 0.753 | 1.829 |

9.5 Summary

Key numerical results in Tables 9.1, 9.2, and 9.3 indicate that, similar to the case with shaking in the longitudinal direction, lateral displacements of the wall facing and settlements and lateral displacements of the bridge seat are small for shaking in the transverse direction, and would likely be considered acceptable for a major earthquake such as Northridge. The results also show that shear keys underneath the bridge seat were effective in reducing settlement and lateral movement of the bridge seat. These values are 0.65 in. and 0.75 in., respectively, and would not generally be expected to cause serious distress to a single-span or multi-span bridge.

Chapter 10 – Conclusions

The following conclusions are based on the foregoing literature review and a numerical study of static and seismic performance of geosynthetic-reinforced soil (GRS) bridge abutments using the FLAC-2D finite difference analysis program:

- For GRS bridge abutments, the bridge load is directly applied to the reinforced soil backfill through a shallow foundation. This design concept represents significant cost savings through the avoidance of deep foundations (piles) to support the bridge and provides several other advantages, including faster and easier construction and reduction of differential settlement between the bridge and approach roadways.
- Although good performance of GRS abutments has been demonstrated for static loading, much less is known with regard to their performance under seismic loading conditions. Additional research and large-scale testing is needed to address these issues before GRS abutments can be used to their full advantage in high seismic areas like California.
- A comparison of measured and predicted displacements for the Founders/Meadows GRS bridge abutment indicates that: (1) static loading displacements for the abutment for both end-of-construction and in-service conditions were small, and (2) FLAC-2D did a good job in predicting these displacements.
- A comparison of measured and predicted displacements for a large-scale seismic shaking test of a field-scale GRS retaining wall indicates that FLAC-2D may overestimate, rather than underestimate, displacements for GRS structures under seismic loading conditions.
- Numerical results indicate that lateral displacements of the wall facing and settlements and lateral displacements of the bridge seat are small for shaking in the longitudinal direction, and would likely be acceptable for a major earthquake such as Northridge. In particular, the value of seismic-induced settlement is estimated to be 0.65 in., which would not generally be expected to cause serious concern for a single-span or multi-span bridge.
- In a side-by-side comparison, FLAC-2D and ABAQUS produced similar values of bridge seat settlement and lateral wall displacement for a GRS-supported bridge subjected to Northridge ground motion in the longitudinal direction. This agreement lends credibility to the other FLAC-2D results presented throughout this report.
- Numerical results indicate that lateral displacements of the wall facing and settlements and lateral displacements of the bridge seat are also small for shaking in the transverse direction, and would likely be acceptable for a major earthquake such as Northridge. Simulation results indicate that the use of shear keys underneath the bridge seat is effective in reducing settlement and lateral movement of the bridge seat due to Northridge ground motion in the transverse direction.

This Phase I study is the first part of a multi-phase research program to investigate the seismic performance of GRS bridge abutments and develop guidelines for seismic design of these structures for Caltrans. Phase I has consisted of literature review and numerical studies, leading up to a Phase II investigation. Phase II will consist of shake table tests on six reduced-scale GRS bridge abutments and FLAC-3D numerical analyses. A Phase II proposal was submitted in fall 2014, with work starting in summer 2015. This experimental work will provide data to (1) indicate the performance of reduced-scale GRS abutment structures under seismic loading, and (2) calibrate numerical models for the simulation of the seismic response of full-scale GRS abutment structures.

REFERENCES

- Abu-Hejleh, N., Outcalt, W., Wang, T., and Zornberg, J.G. (2000). *Performance of Geosynthetic-Reinforced Walls Supporting the Founders/Meadows Bridge and Approaching Roadway Structures, Report 1: Design, Materials, Construction, Instrumentation, and Preliminary Results*. Report No. CDOT-DTD-R-2000-5, Colorado Department of Transportation, Colorado, USA.
- Abu-Hejleh, N., Zornberg, J.G., Wang, T., McMullen, M., and Outcalt, W. (2000). *Performance of Geosynthetic-Reinforced Walls Supporting the Founders/Meadows Bridge and Approaching Roadway Structures, Report 2: Assessment of the Performance and Design of the Front GRS Walls and Recommendations for Future GRS Abutments*. Report No. CDOT-DTD-R-2001-12, Colorado Department of Transportation, Colorado, USA.
- Abu-Hejleh, N., Zornberg, J.G., Wang, T., and Watcharamonthein, J. (2001). "Monitored displacements of unique geosynthetic-reinforced soil bridge abutments." *Geosynthetics International*, 9(1), 71-95.
- Adams, M. (1997). "Performance of a prestained geosynthetic reinforced soil bridge pier." *Mechanically Stabilized Backfill*, Balkema, Rotterdam, Netherland, 35-53.
- Adams, M., Nicks, J., Stabile, T., Wu, J., Schlatter, W., and Hartman, J. (2011). *Geosynthetic Reinforced Soil Integrated Bridge System Synthesis Report*, FHWA-HRT-11-027, U.S. Department of Transportation, Washington, D.C.
- Allen, T. M. (2011). "AASHTO Seismic Design Specifications for Walls – Key Changes Proposed for 2011." Presentation, May 5, 2011.
- Bachus, R.C., Fragazy, R.J., Jaber, M., Olem, K.L., Yuan, Z., and Jewell, R., (1992). *Dynamic response of reinforced soil systems*. USAF Research Report F0 8635-90-C-0198, Vol. 1 & 2, Air Force Civil Engineering Support Agency, Florida, USA.
- Bathurst, R.J. (2006). "Reinforced Soil Retaining Wall Testing, Modeling and Design." *12'th Indian Geotechnical Conference*, Madras, India, 21-32.
- Bathurst, R.J., and Hatami, K. (1998). "Seismic response analysis of a geosynthetic reinforced soil retaining wall." *Geosynthetics International*, 5(1-2), 127-166.
- Bathurst, R.J., and Hatami, K. (1999). "Numerical study of the influence of base shaking on geosynthetic reinforced retaining walls." *Geosynthetics '99*, Boston, MA, USA, 2, 963-976.
- Bathurst, R.J., and Hatami, K. (2006a). "Parametric analysis of reinforced soil walls with different height and reinforcement stiffness." *8th International Conference on Geosynthetics*, Yokohama, Japan, 1343-1346.
- Bathurst, R.J., and Hatami, K. (2006b). "Physical to computational modelling of reinforced soil walls under static loading." *2nd International Conference on Physical Modeling in Geotechnics*, Hong Kong, China, 1, 3-17.
- Bathurst, R.J., Huang, B., and Hatami, K. (2008). "Numerical modeling of geosynthetic reinforced retaining walls." *12th International Conference of the International Association for Computer Methods and Advances in Geomechanics (IACMAG)*, Goa, India, 4071-4080.

- Bathurst, R.J., Karpurapu, R.G. and Jarrett, P.M. (1992). "Finite Element Analysis of a Geogrid Reinforced Soil Wall." *ASCE GSP 30: Grouting, Soil Improvement and Geosynthetics*, 2, 1213-1224.
- Bathurst, R.J., Nernheim, A., Walters, D.L., Allen, T.M., Burgess, P. and Saunders, D. (2009). "Influence of Reinforcement Stiffness and Compaction on the Performance of Four Geosynthetic Reinforced Soil Walls." *Canadian Geotechnical Journal*, 16(1), 43-59.
- Bathurst, R.J., Vlachopoulos, N., Walters, D.L., Burgess, P.G. and Allen, T.M. (2006). "The influence of facing rigidity on the performance of two geosynthetic reinforced soil retaining walls." *Canadian Geotechnical Journal*, 43(12), 1225-1237.
- Bathurst, R.J., Walters, D., Vlachopoulos, V., Burgess, P., and Allen, T.M. (2000). "Full scale testing of geosynthetic reinforced walls." *Advances in Transportation and Geoenvironmental Systems using Geosynthetics, GeoDenver 2000*, Denver, Colorado, USA, 201-217.
- Berg, R.R., Christopher, B.R., and Samtani, N.C. (2009). *Design and Construction of Mechanically-Stabilized Earth Walls and Reinforced Soil Slopes – Volume I*. Publication No. FHWA-NHI-10-024, FHWA, U.S. Department of Transportation, Washington, D.C., USA.
- Cai, Z., and Bathurst, R.J. (1995). "Seismic response analysis of geosynthetic reinforced soil segmental retaining walls by finite element method." *Computers and Geotechnics*, 17(4), 523-546.
- Chida, S., Minami, K., and Adachi. (1985). "Tests with regard to the stability of the fill constructed by the reinforced earth technique." 13p. (unpublished report translated from Japanese)
- Collin, J. G., Chouery-Curtis, V. E., and Berg, R. R. (1992). "Field observation of reinforced soil structures under seismic loading." *Earth Reinforcement Practice*, 1, 223–228, A.A. Balkema, Netherlands.
- Duncan, J.M., Byrne, P., Wong, K.S., and Mabry, P. (1980). *Strength, stress-strain and bulk modulus parameters for finite element analysis of stresses and movements in soil masses*. Report No. UCB/GT/80-01, University of California, Berkeley, CA, USA.
- Earth Mechanics, Inc. (2005). *Field Investigation Report for Abutment Backfill Characterization*. Report No. SSRP-05/02, California Department of Transportation (Caltrans), CA, USA.
- El-Emam, M., and Bathurst, R.J. (2004). "Experimental design, instrumentation and interpretation of reinforced soil wall response using a shaking table." *International Journal of Physical Modelling in Geotechnics*, 4(4), 13-32.
- El-Emam, M., and Bathurst, R.J. (2005). "Facing contribution to seismic response of reduced-scale reinforced soil walls." *Geosynthetics International*, 12(5), 215-238.
- El-Emam, M., and Bathurst, R.J. (2007). "Influence of reinforcement parameters on the seismic response of reduced-scale reinforced soil retaining walls." *Geotextiles and Geomembranes*, 25(1), 33-49.

- El-Emam, M., Bathurst, R.J., and Hatami, K. (2004). "Numerical modeling of reinforced soil retaining walls subjected to base acceleration." *13th World Conference on Earthquake Engineering*, Vancouver, BC, Canada, Paper No. 2621.
- Fakharian, K., and Attar, I.H. (2007). "Static and seismic numerical modeling of geosynthetic-reinforced soil segmental bridge abutments." *Geosynthetics International*, 14(4), 228-243.
- Gotteland, P., Gourc, J.P., and Villard, P. (1997). "Geosynthetic reinforced structures as bridge abutments: Full scale experimentation and comparison with modelisations." *Mechanically Stabilized Backfill*, Balkema, Rotterdam, Netherland, 25-34.
- Hatami, K., and Bathurst, R.J. (2000a). "Effect of structural design on fundamental frequency of reinforced-soil retaining walls." *Soil Dynamics and Earthquake Engineering*, 19(3), 137-157.
- Hatami, K., and Bathurst, R.J. (2000b). "Investigation of seismic response of reinforced soil retaining walls." *4th International Conference on Recent Advances in Geotechnical Earthquake Engineering and Soil Dynamics*, San Diego, CA, USA, Paper No. 7.18.
- Hatami, K., and Bathurst, R.J. (2005a). "Development and verification of a numerical model for the analysis of geosynthetic reinforced soil segmental walls under working stress conditions." *Canadian Geotechnical Journal*, 42(4), 1066-1085.
- Hatami, K., and Bathurst, R.J. (2005b). "Verification of a numerical model for reinforced soil segmental retaining walls." *Geofrontiers 2005: Slopes and Retaining Structures under Seismic and Static Conditions*, Austin, Texas, USA.
- Hatami, K., and Bathurst, R.J. (2005c). "Parametric analysis of reinforced soil walls with different backfill material properties." *North American Geosynthetics Society 2005 Conference*, Las Vegas, Nevada, USA.
- Hatami, K., and Bathurst, R.J. (2006). "Numerical model for reinforced soil segmental walls under surcharge loading." *Journal of Geotechnical and Geoenvironmental Engineering*, 132(6), 673-684.
- Helwany, S.M.B., Budhu, M., and McCallen, D. (2001). "Seismic analysis of segmental retaining walls. I: Effects of facing details." *Journal of Geotechnical and Geoenvironmental Engineering*, 127(9), 750-756.
- Helwany, S.M.B., and McCallen, D. (2001). "Seismic analysis of segmental retaining walls. II: Model verification." *Journal of Geotechnical and Geoenvironmental Engineering*, 127(9), 741-749.
- Helwany, S.M.B., Reardon, G., and Wu, J.T.H. (1999). "Effects of backfill on the performance of GRS retaining walls." *Geotextiles and Geomembranes*, 17, 1-16.
- Helwany, S.M.B., Wu, J.T.H., and Froessl, B. (2003). "GRS bridge abutments – an effective means to alleviate bridge approach settlement." *Geotextiles and Geomembranes*, 21, 177-196.
- Helwany, S.M.B., Wu, J.T.H., and Kitsabunnarat, A. (2007). "Simulating the behavior of GRS bridge abutments." *Journal of Geotechnical and Geoenvironmental Engineering*, 133(10), 1129-1240.

- Helwany, S.M.B., Wu, J.T.H., and Meinholz, P. (2012). *Seismic Design of Geosynthetic-Reinforced Soil Bridge Abutments with Modular Block Facing*. NCHRP Web-Only Document 187, Transportation Research Board, Washington, D.C., USA.
- Ho, S.K., and Rowe, R.K. (1997). "Effect of wall geometry on the behaviour of reinforced soil walls." *Geotextiles and Geomembranes*, 14(10), 521-541.
- Huang, B., Bathurst, R.J., and Hatami, K. (2009). "Numerical study of reinforced soil segmental walls using three different constitutive soil models." *Journal of Geotechnical and Geoenvironmental Engineering*, 135(10), 1486-1498.
- Huang, B., Bathurst, R.J., Hatami, K., and Allen, T.M. (2010). "Influence of toe restraint on reinforced soil segmental walls." *Canadian Geotechnical Journal*, 47(8), 885-904.
- Ingold, T.S. (1982). *Reinforced Earth*. Thomas Telford Ltd., London.
- Itasca Consulting Group, Inc. (2011). "Fast Lagrangian Analysis of Continua – 2D, Version 7.0." Itasca Consulting Group, Inc., Minneapolis, MN, USA.
- Jones, C.J.F.P. (1996). *Earth reinforcement & soil structures*. Thomas Telford Ltd.
- Karpurapu, R.G., and Bathurst, R.J. (1995). "Behaviour of geosynthetic reinforced soil retaining walls using the finite element method." *Computers and Geotechnics*, 17(3), 279-299.
- Ketchart, K., and Wu, J.T.H. (1997). "Performance of geosynthetic-reinforced soil bridge pier and abutment, Denver, Colorado, USA." *Mechanically Stabilized Backfill*, Balkema, Rotterdam, Netherland, 101-116.
- Koseki, J. (2012). "Use of geosynthetics to improve seismic performance of earth structures," *Geotextiles and Geomembranes*, 34, 51-68.
- Koseki, J., Bathurst, R. J., Guler, E., Kuwano, J., and Maugeri, M. (2006). "Seismic stability of reinforced soil walls." *8th International Conference on Geosynthetics*, Yokohama, Japan.
- Koseki, J., Munaf, Y., Tatsuoka, F., Tateyama, M., Kojima, K., and Sato, T. (1998). "Shaking and tilt table tests of geosynthetic-reinforced soil and conventional-type retaining walls." *Geosynthetics International*, 5(1-2), 73-96.
- Krishna, A.M., and Latha, G.M. (2009). "Seismic behavior of rigid-faced reinforced soil retaining wall models: reinforcement effect." *Geosynthetics International*, 16(5), 364-373.
- Latha, G.M., and Krishna, A.M. (2008). "Seismic response of reinforced soil retaining wall models: Influence of backfill relative density." *Geotextiles and Geomembranes*, 26, 335-349.
- Lee, K. L., Adams, B., and Vagneron, J. (1973). "Reinforced earth retaining walls," *Journal of the Soil Mechanics and Foundations Division*, ASCE, 99(10), 745-764.
- Lee, K.Z.Z., and Chang, N.Y. (2012). "Predictive modeling on seismic performances of geosynthetic-reinforced soil walls." *Geotextiles and Geomembranes*, 35, 25-40.
- Lee, K.Z.Z., Chang, N.Y., and Ko, H.Y. (2010). "Numerical simulation of geosynthetic-reinforced soil walls under seismic shaking." *Geotextiles and Geomembranes*, 28, 317-334.
- Lee, W. (2000). *Internal Stability of Analyses of Geosynthetic Reinforced Retaining Walls*." Ph.D. Thesis, University of Washington, Seattle, USA.

- Leshchinsky, D, and Vulova, C. (2001). "Numerical investigation of the effects of geosynthetic spacing on failure mechanisms in MSE block walls." *Geosynthetics International*, 8(4), 343-365.
- Ling, H.I. (2005). "Finite element applications to reinforced soil retaining walls – simplistic versus sophisticated analyses." ASCE GSP 143: *Geomechanics: Testing, Modeling and Simulation*, 217-236.
- Ling, H.I., Cardany, C., Sun, L-X., and Hashimoto, H. (2000). "Finite element analysis of a geosynthetic-reinforced soil retaining wall with concrete-block facing." *Geosynthetics International*, 7(2), 137-162.
- Ling, H.I., and Leshchinsky, D. (2003). "Finite element parametric studies of the behavior of segmental block reinforced soil retaining walls." *Geosynthetics International*, 10(3), 77-94.
- Ling, H.I., Leshchinsky, D., and Chou, N.N.S. (2001). "Post-earthquake investigation on several geosynthetic-reinforced soil retaining walls and slopes during the Ji-Ji earthquake of Taiwan," *Soil Dynamics and Earthquake Engineering*, 21, 297-313.
- Ling, H.I., Leshchinsky, D., Mohri, Y., and Wang, J. (2012). "Earthquake response of reinforced segmental retaining walls backfilled with substantial percentage of fines." *Journal of Geotechnical and Geoenvironmental Engineering*, 138(8), 934-944.
- Ling, H.I., Liu, H., Kaliakin, V., and Leshchinsky, D. (2004). "Analyzing dynamic behavior of geosynthetic-reinforced soil retaining walls." *Journal of Engineering Mechanics*, 130(8), 911-920.
- Ling, H.I., Mohri, Y., Leshchinsky, D., Burke, C., Matsushima, K., and Liu, H. (2005a). "Large scale shaking table tests on modular block reinforced soil retaining wall." *Journal of Geotechnical and Geoenvironmental Engineering*, 131(4), 465-476.
- Ling, H.I., Liu, H., and Mohri, Y. (2005b). "Parametric studies on the behavior of reinforced soil retaining walls under earthquake loading." *Journal of Engineering Mechanics*, 131(10), 1056-1065.
- Ling, H.I., Yang, S., Leshchinsky, D., Liu, H., and Burke, C. (2010). "Finite-element simulations of full-scale modular-block reinforced soil retaining walls under earthquake loading." *Journal of Engineering Mechanics*, 136(5), 653-661.
- Liu, H., Wang, X., and Song, E. (2010). "Centrifuge testing of segmental geosynthetic-reinforced soil retaining walls subjected to modest seismic loading." *GeoFlorida 2010: Advanced in Analysis, Modeling & Design*, Florida, USA, 2992-2998.
- Lostumbo, J.M., and Artieres, O. (2011). "Geosynthetic enabled with fiber optic sensors for MSE bridge abutment supporting shallow bridge foundation," *Proceedings, Geo-Frontiers 2011*, ASCE, 3497-3504.
- Matsuo, O., Tsutsumi, T., Yokoyama, K., and Saito, Y. (1998). "Shaking table tests and analyses of geosynthetic-reinforced soil retaining walls." *Geosynthetics International*, 5(1-2), 97-126.
- Mitchell, J.K., and Christopher, B.R. (1990). "North American practice in reinforced soil systems," *Design and Performance of Earth Retaining Structures*, GSP No. 25, ASCE, 332-346.

- Richardson, G.N., Feger, D., Fong, A., and Lee, K.L. (1977). "Seismic testing of reinforced earth walls." *Journal of Geotechnical Engineering Division*, 103(1), 1–17.
- Richardson, G.N., and Lee, K.L. (1975). "Seismic design of reinforced earth walls." *Journal of Geotechnical Engineering Division*, 101(2), 167–188.
- Rowe, R.K., and Ho, S.K. (1997). "Continuous panel reinforced soil walls on rigid foundations." *Journal of Geotechnical and Geoenvironmental Engineering*, 123(10), 912-920.
- Rowe, R.K., and Ho, S.K. (1998). "Horizontal deformation in reinforced soil walls." *Canadian Geotechnical Journal*, 35(2), 312-327.
- Runser, D., Fox, P. J., and Bourdeau, P. L. (2001). "Field performance of a 17 m-high reinforced soil retaining wall." *Geosynthetics International*, 8(5), 367-391
- Sakaguchi, M. (1996). "A study of the seismic behaviour of geosynthetic reinforced walls in Japan." *Geosynthetics International*. 3(1), 13–40.
- Schlosser, F., and Bastick, M. (1991). Reinforced Earth, *Foundation Engineering Handbook, 2nd ed.*, H.-Y. Fang, ed., Chapman & Hall, New York, 778-795.
- Schlosser, F., and Elias, V. (1979). "Friction in reinforced earth," *Proceedings, Symposium on Earth Reinforcement*, ASCE Annual Convention, Pittsburg, PA, 735-762.
- Segrestin, P., and Bastick, M. (1988). "Seismic design of reinforced earth retaining wall – the contribution of finite element analysis." *International Geotechnical Symposium on Theory and Practice of Earth Reinforcement*, Fukuoka, Kyushu, Japan, 577-582.
- Siddharthan, R.J., Ganeshwara, V., Kutter, B.L., El-Desouky, M., and Whitman, R.V. (2004). "Seismic deformation of bar mat mechanically stabilized earth walls. I: Centrifuge tests." *Journal of Geotechnical and Geoenvironmental Engineering*, 130(1), 14-25.
- Skinner, G.D., and Rowe, R.K. (2005). "Design and behavior of a geosynthetic reinforced retaining wall and bridge abutment on a yielding foundation." *Geotextiles and Geomembranes*, 23, 234-260.
- Stein, W.J., and Neuman, T.R. (2007). *Mitigation Strategies for Design Exceptions*. FHWA-SA-07-011, Federal Highway Administration, Washington, D.C., USA.
- Takemura, J., and Takahashi, A. (2003). "Centrifuge modeling of seismic performance of reinforced earth structure." *Reinforced soil engineering: Advances in research and practice*, H. I. Ling, D. Leshchinsky, and F. Tatsuoka, eds., Marcel Dekker, New York, 417–442.
- Tatsuoka, F. (2008). "Recent practice and research of geosynthetic-reinforced earth structures in Japan," *Journal of GeoEngineering*, 3(3), 77-100.
- Tatsuoka, F., Koseki, J., and Tateyama, M. (1996). "Performance of reinforced soil structures during the 1995 Hyogo-ken Nanbu Earthquake," *Earth Reinforcement*, Special Report, pp. 1–36, A.A. Balkema, The Netherlands.
- Vidal, H. (1969). "The principle of reinforced earth," *Highway Research Record*, 282(1659), 1-16.
- Vucetic, M., Tufenkjian, M. R., Felio, G. Y., Barar, P., and Chapman, K. R. (1998). "Analysis of soil-nailed excavations stability during the 1989 Loma Prieta Earthquake," *The Loma Prieta, California, Earthquake of October 17, 1989—Earth Structures and Engineering*

- Characterization of Ground Motion*, Professional Paper 1552-D, United States Geological Survey, Washington, DC.
- Wu, J.T.H., Ketchart, K., and Adams, M. (2001). *GRS Bridge Piers and Abutments*. Report No. FHWA-RD-00-038, FHWA, U.S. Department of Transportation, Washington, D.C., USA.
- Wu, J.T.H., Lee, K.Z.Z, Helwany, S.B., and Ketchart, K. (2006a). *Design and Construction Guidelines for Geosynthetic-Reinforced Soil Bridge Abutments with a Flexible Facing*. NCHRP Report 556, Transportation Research Board, Washington, D.C., USA.
- Wu, J.T.H., Lee, K.Z.Z, and Pham, T. (2006b). "Allowable bearing pressures of bridge sills on GRS abutments with flexible facing." *Journal of Geotechnical and Geoenvironmental Engineering*, 132(7), 830-841.
- Yen, W.-H. P., Chen, G., Buckle, I., Allen, T., Alzamora, D., Ger, J., and Arias, J. G. (2011). *Post-Earthquake Reconnaissance Report on Transportation Infrastructure: Impact of the February 27, 2010, Offshore Maule Earthquake in Chile*, FHWA-HRT-11-030, U.S. Department of Transportation, Washington, D.C.
- Yogendrakumar, M., and Bathurst, R.J. (1992). "Numerical simulation of reinforced soil structures during blast loadings." *Transportation Research Record* 1336, 1-8.
- Yogendrakumar, M., Bathurst, R.J., and Finn, W.D.L. (1991). "Response of reinforced soil walls to earthquake loads." *IX Panamerican Conference on Soil Mechanics and Foundation Engineering*, Vina del Mar, Chile, 659-672.
- Yogendrakumar, M., Bathurst, R.J. and Finn, W.D.L. (1992). "Dynamic response analysis of a reinforced soil retaining wall." *Journal of Geotechnical Engineering*, 118(8), 1158-1167.
- Zarnani, S., and Bathurst, R.J. (2009). "Influence of constitutive model on numerical simulation of EPS seismic buffer shaking table tests," *Geotextiles and Geomembranes*, 27, 308-312.
- Zevgolis, I, and Bourdeau, P.L. (2007). *Mechanically Stabilized Earth Wall Abutments for Bridge Support*. Publication No. FHWA/IN/JTRP-2006/38, Indiana Department of Transportation and Purdue University, West Lafayette, IN, USA.
- Zornberg, J.G., Abu-Hejleh, N., and Wang, T. (2001). "Geosynthetic-reinforced soil bridge abutments. Measuring the performance of geosynthetic reinforcement in a Colorado bridge structure." *GFR*, 19(2), 7 p.